Marine Geology 462 (2023) 107099

Contents lists available at ScienceDirect

Marine Geology

journal homepage: www.elsevier.com/locate/margo

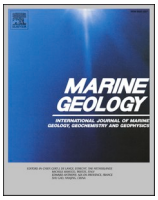

Research Article

Morphosedimentary characteristics and formation mechanisms of new beaches generated after the Tajogaite volcano eruption of 2021 (La Palma, Spain)

Ignacio Alonso [a,*], Francisco J. Santana-Sarmiento [b], Flora Andrés-Araujo [b], Mariona Casamayor [c], Isabel Montoya-Montes [a,d], Alex Brenes [a], Rogelio Herrera [e], María J. Sánchez-García [a]

[a] Instituto de Oceanografía y Cambio Global (IOCAG), Universidad de Las Palmas de Gran Canaria, Campus de Tafira, 35017 Las Palmas, Spain
[b] Departamento de Cartografía y Expresión Gráfica en la Ingeniería, Universidad de Las Palmas de Gran Canaria, Campus de Tafira, 35017 Las Palmas, Spain
[c] Plataforma Oceánica de Canarias (PLOCAN), Carretera de Taliarte s/n, 35200 Telde, Spain
[d] Instituto Geológico y Minero de España (IGME-CSIC), Unidad Territorial de Canarias, c/Alonso Alvarado 43, 2A, 35003 Las Palmas, Spain
[e] Servicio de Biodiversidad, Consejería para la Transición Ecológica, Lucha contra el Cambio Climático y Planificación Territorial, Gobierno de Canarias, Las Palmas, Spain

ARTICLE INFO

Editor: Edward Anthony

Keywords:
Lava delta
Beachface slope
Run-up
Textural maturity
Wave storms
Wave steepness
Onshore transport

ABSTRACT

Only in very special circumstances can new beaches develop due to natural processes in areas where they did not exist before. One such circumstance is related to volcanic eruptions, when a lava flow reaches the ocean. The sudden formation of new beaches is examined in this paper. Following the Tajogaite volcano eruption in September 2021, two lava deltas formed after the arrival of several lava flows to the coast. Attached to the flanks and front of these lava deltas, thirteen gravel beaches formed in just a few months. Detailed topographic and sedimentologic information was collected both on the beaches and adjacent submarine areas. The volume of sediments accumulated on these beaches was obtained after comparison of the actual topography with a previous one, yielding a total net accumulation of about 79,000 m^3 of volcanoclastic pebbles and cobbles. This material comes from two major source areas: extensive offshore deposits of volcanic clasts within the depth of closure which are moved onshore by low steepness swell waves, and rock fragments derived from erosion of the lava delta front by high energy waves. Two types of beaches were identified. Beaches that already existed prior to the eruption showed significant increases in cross-shore length and height, with a net accumulation of 67,000 m^3. In contrast, the dismantling of the lava delta front led to the formation of totally new beaches in certain locations, accounting for about 12,000 m^3 of sediments. Several features, such as a steep foreshore slope, a well-developed storm berm and the presence of wood debris in many of these beaches at several meters height and tens of meters inland, are examined conjointly with the sediment characteristics, showing how textural maturity can change in response to the forcing agents acting in the different parts of the beach profile. The future evolution of these beaches is also considered. This study can enrich the knowledge regarding how new gravel beaches can form in volcanic settings.

1. Introduction

After several days of seismicity and ground deformation, a volcanic eruption began on La Palma (Canary Islands, Spain) at 14:05 (UTC) on 19 September 2021. The initial cone emerged in the Cabeza de Vaca area, not far from the eruptive center of the San Juan eruption in 1949, on the western flank of the Cumbre Vieja ridge. The eruption lasted until 13 December 2021, though it was not officially declared over until 25 December. During this period huge amounts of volcanic materials (gases, lava flows and tephra) were produced.

The eruption was La Palma's longest and most voluminous (>200 million m^3) in historical times (González, 2022). As a result, a new pyroclastic monogenetic cone of about 200 m high was formed, several lava flows extended over around 1100 ha and volcanic ash was

* Corresponding author.
E-mail address: ignacio.alonso.bilbao@ulpgc.es (I. Alonso).

https://doi.org/10.1016/j.margeo.2023.107099
Received 25 March 2023; Received in revised form 12 June 2023; Accepted 30 June 2023
Available online 7 July 2023

distributed over the whole island, even reaching the neighboring islands of Tenerife and El Hierro. The eruption severely affected numerous villages, infrastructures (mostly roads and water irrigation systems), pine forest areas and the main economic engine of the island, banana cultivation. The eruption also impacted the marine environment, with physical-chemical and biological alterations of coastal seawater (Román et al., 2022).

The successive lava flows that occurred mainly comprised trachybasalt rocks emitted as A'a-type and pahoehoe-type lava flows (Palanco et al., 2022). The flows descended towards the coast and reached the ocean at two spots, with two lava deltas being formed, both of which have an overall lobate morphology (Fig. 1). The southernmost lava delta, with a total extension of 76 ha, began to develop on 29 September and was fed by several lava flows during nearly 2 months. Some 33 ha of that extension overlaps a former lava delta from the San Juan volcano eruption of 1949, while the remaining 43 ha correspond to coastal progradation, indicating that this part of the lava delta occupies an area previously covered by the ocean. Román et al. (2022) reported an approximate total volume of 5×10^6 m^3 in the lava delta, with a higher accumulation of lava attached to the former cliff and abrupt lobes observed on the flanks. The northernmost lava delta was formed during the final stages of the eruption, resulting from a lava flow reaching the ocean on 01 December. It is much smaller, accounting for just 5 ha of coastal progradation and also has a generally lobate morphology and abrupt flanks.

The fronts of the lava deltas are irregularly shaped and highly indented. Several beaches formed at different locations along the fronts of both lava deltas in the lapse of a few months. This is one of the rare cases in which new beaches are exclusively formed due to natural processes, without the intervention of any human activity. In this context, the role of volcanic activity when a lava flow reaches the ocean leading to the formation of new beaches is examined in the paper. The aim of this work is to provide information about the topographic and sedimentologic characteristics of these newly formed beaches, to estimate the volume of material involved, and to analyze the different mechanisms that could have led to their formation.

2. Study area

La Palma is the second youngest island of the Canary Archipelago. Located above the theoretical hotspot in the NW of the Canary Islands (Spain), it dates back to 1.8 Ma and its origin is associated to volcanism. It has a terrestrial surface area of 706 km^2, a coastline of 180 km and its highest point is 2426 m above sea level (Carracedo et al., 2001). The island is the subaerial expression of a 6400 m high oceanic volcano emplaced on oceanic crust of the Jurassic age (Banda et al., 1981). The submarine stage of the development of the island (Seamount series) is observed within the lower part of Caldera de Taburiente (Carracedo et al., 2001).

The oldest subaerial volcanism can be seen in the northern sector of the island where large lateral collapses have taken place (Ancochea et al., 1994; Carracedo et al., 2001). Following formation of the Garafía and Taburiente volcanic edifices (Fig. 1), the eruptive activity moved southwards leading to the formation of the Cumbre Nueva rift. The

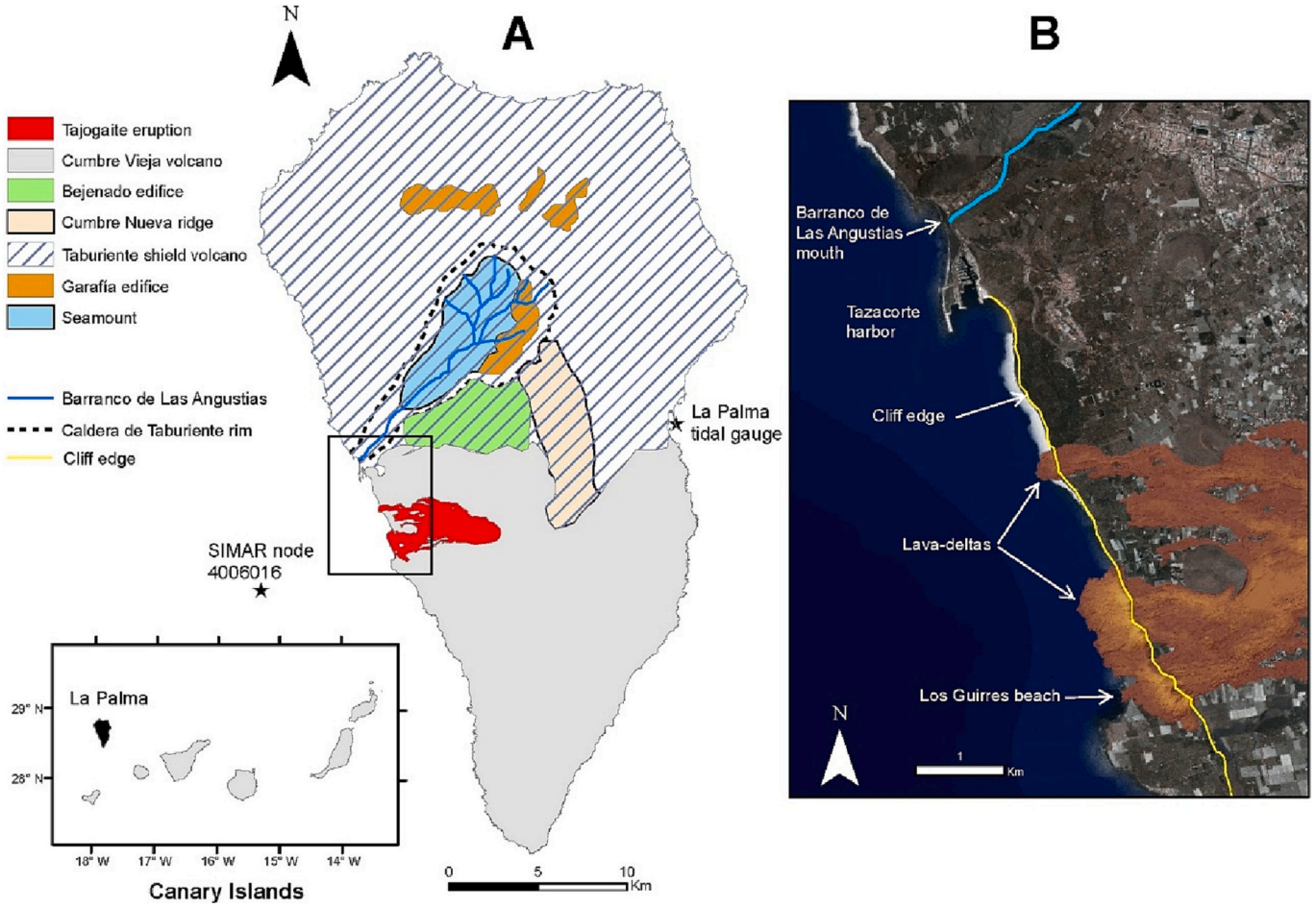

Fig. 1. A) Simplified geomorphological map of La Palma Island showing the most important geological and geomorphological features and the source of oceanographic data. B) Inset of the study area showing the location of both lava deltas at the most distal part of the 2021 eruption. Orthophoto obtained from https://www.opendatalapalma.es/

progressive growth of the Cumbre Nueva rift resulted in structural instability of the whole ridge, triggering a gravitational landslide of the western flank, named the Cumbre Nueva Debris Avalanche, and the detachment of some 95 km^3 (Urgeles, 1999). These materials, detectable using swath bathymetry, reach depths of up to 4000 m along the submarine part of the island edifice (Masson et al., 2002). As a result of this giant gravitational flank collapse, a wide depression was formed (Valle de Aridane), which was partially filled with new lava flows from the Bejenado edifice, and formation began of the Caldera de Taburiente through incision and retrogressive erosion (Carracedo et al., 2001).

The latter volcanic period resulted in the formation of the Cumbre Vieja rift, a nearly 2000 m high topographic ridge elongated in a N-S direction. It has rapidly grown over the past 123 kyr (Carracedo et al., 2001), resulting in steep-sided volcano flanks. The historic eruptive activity has been concentrated in the Cumbre Vieja ridge, with the last three eruptions being those of San Juan in 1949, Teneguía in 1971 and the 2021 event.

The Caldera de Taburiente is the largest erosive caldera in the Canary Islands. The eroded materials are washed away through the Barranco de Las Angustias gully, which has a funnel-like morphology with a wide head and a riverbed that gradually narrows until it ends at Tazacorte beach (Fig. 2A). Considering *(i)* the length of this gully (15 km), *(ii)* the height difference between its head and mouth (2400 m), *(iii)* the catchment area (around 55 km^2), and *(iv)* the rainfall regime (900 mm/year on average, although heavy rain events of >200 mm/day have been recorded), it is possible to understand the rapid development of Tazacorte beach as the result of the input of sediments from the basin (Marrero et al., 2017).

The western flank of the Cumbre Vieja rift presents steep slopes and is generally uniform with only slight ravine incisions. More than ten volcanic cones interrupt the smooth slopes which end at coastal cliffs. Cliff height ranges from between 50 m in the area close to Tazacorte harbor to 130 m at Los Guirres beach (Fig. 1). The cliffs are highly vertical and rockfalls are frequent (Fig. 2B). At certain locations, these cliffs have been covered by lava flows from the different eruptions generated after formation of the Cumbre Vieja volcano (Fig. 2C). At these locations, cliff verticality is smoothed, and coastal platforms can be found at the base of the cliff. Found along the SW coastline of La Palma is a 7.4 km long coastal platform that originated from the San Juan volcano eruption (Carracedo et al., 2001). Its maximum width of 1.1 km is found south of Los Guirres beach. Several beaches formed by volcanic sand, gravel and pebbles are located along this coastal platform.

The coast of La Palma, like the rest of the Canary Islands, is under the

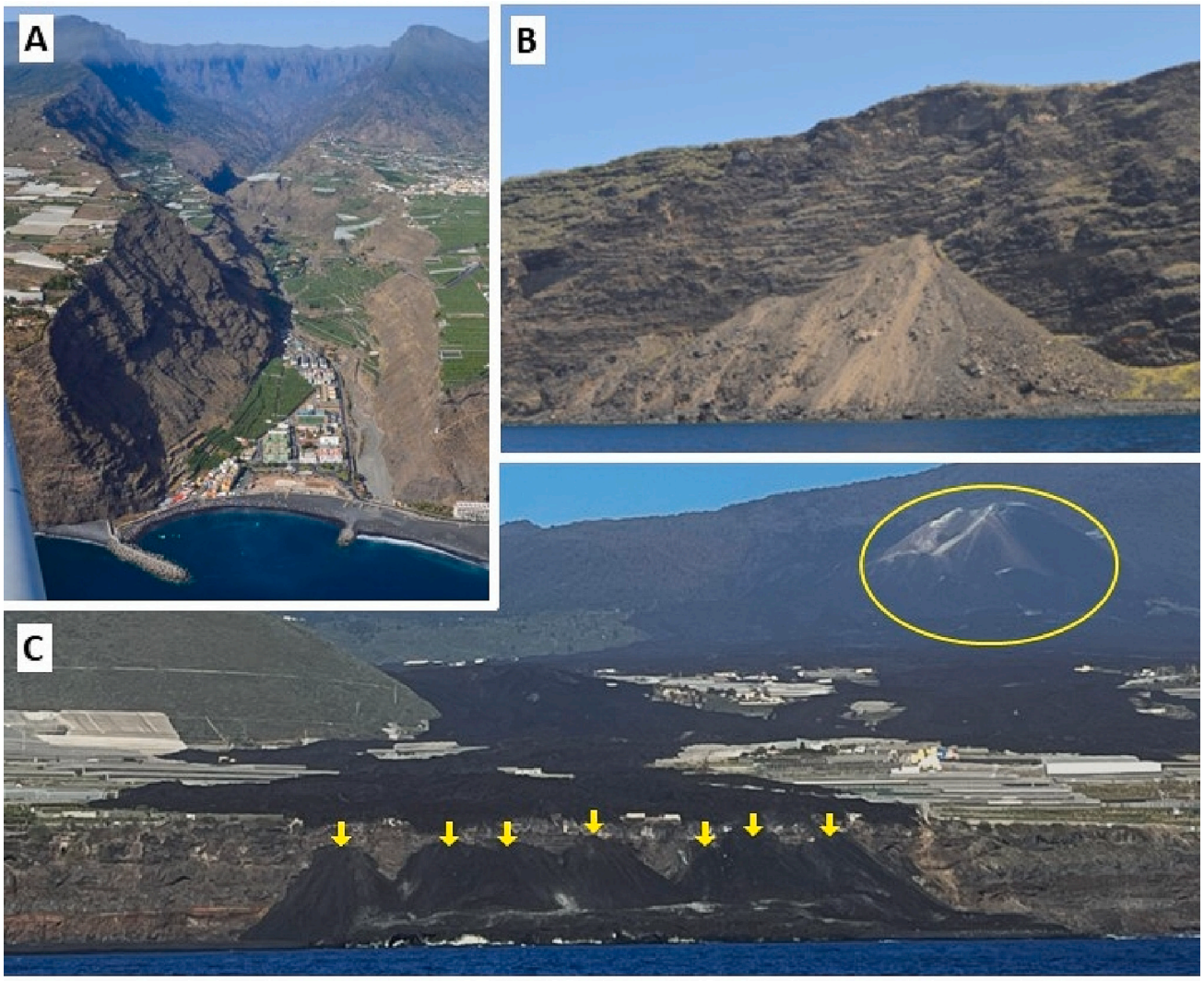

Fig. 2. A) Aerial view of Barranco de Las Angustias from its mouth. This is the only draining area for all the water collected in the Caldera de Taburiente. Note the deeply set bed. B) Nearly vertical cliffs and associated rockfalls in the western coast of La Palma. C) Photograph from the ocean of the lava flow and the northern lava delta generated after the 2021 Tajogaite eruption. The places where the lava fell from the cliff edge are marked with arrows. The pyroclastic cone formed after the eruption is highlighted in yellow in the top right-hand corner of the image.

influence of NNE-NE trade winds most of the year. The islands are usually affected by moderate waves from a NNE direction, with an annual average significant wave height (H_s) of 1.4 m and a spectral peak period (T_p) of 9.5 s. The wave climate presents a strong seasonal pattern, with higher and larger waves in winter compared to those in summer. According to data obtained from the Spanish Ports Authority (Puertos del Estado, 2022), this seasonality in the western part of La Palma includes a 3.48% occurrence of $H_s \geq 4$ m in winter (Dec-Feb) compared to just 0.54% in summer (June-Aug). A similar pattern can be seen in the wave period data, with a 13% occurrence of swell waves of $T_p \geq 16$ s in winter compared to just 0.6% in summer. The tidal regime is characterized by spring and neap ranges of 2.7 m and 0.7 m, respectively (Puertos del Estado, 2019).

The formation of two lava deltas after Tajogaite eruption resulted in the modification of 4 previously existing beaches and the formation of nine new ones. Three of these beaches correspond to the northern lava delta (beaches N2 – N4) and ten to the southern one (beaches S1 - S10). In addition, a beach that existed prior to the eruption and not directly affected by the formation of the lava deltas was also measured as a reference beach. This beach is situated N of the northernmost lava delta (beach N1) (Fig. 3).

3. Data and methods

3.1. In situ data acquisition and processing

Topographic and sedimentological data of the different beaches formed on both lava deltas were collected between 7 and 9 May 2022. The task was not easy, mainly for two reasons: *(i)* access was by means of a rubber boat, but vigorous wave action that could put the boat at risk meant that special care had to be taken when landing or boarding, and *(ii)* as lava flows were still in the degasification process special attention had to be paid to wind direction to prevent direct impact from the gases. Despite these limitations, the collection of sediment and topographic data was performed on the fourteen beaches shown in Fig. 3.

Two Leica DGPS systems model GS09 were simultaneously employed at each site to record the topographic data. For this, the Stop&Go method was used, with observations recorded during a minimum of 5 s at each location. The cartographic reference system was REGCAN95/ UTM zone 28 (EPSG code 4083). Vertical accuracy was 20 mm + 1 ppm (rms). Considering the GNSS station was at a distance of 20 km, the associated uncertainty was 0.04 m. Although it would have been desirable to perform the measurements only at low tide to obtain the largest possible beach extension, this was not possible due to the aforementioned restrictions. However, neap tides did take place during the days of the field survey and therefore tide height was not a major issue. A cloud of topographic points was measured along and across each of the beaches, which was denser in areas with abrupt slope changes (e.g., berm crest or beach cusps) and more spacious in areas with more homogeneous topography (Fig. 3). The onshore limit of topographic data acquisition was the surrounding lava flow or the cliff in those beaches attached to it, while the seaward limit was the shoreline. It was not possible to measure beyond that mark because of the difficulty of standing with the DGPS in a very steep foreshore of coarse clasts under wave action.

Digital elevation models (DEMs) for each beach were generated from the topographic data with QGIS using TIN (Triangulated Irregular Network) methodology with linear interpolation. DEM resolution was 0.1 m and DEM error is 0.04 m, assuming that the TIN model uncertainty was the maximum uncertainty of node points (Fan et al., 2014). Several

	Beach	Area (m^2)	Points Num	Density (pt/m^2)	New beach
Delta North	N1	1658	303	0,18	NO
	N2	4057	596	0,15	NO
	N3	2834	332	0,12	YES
	N4	88	30	0,34	YES
Delta South	S1	4245	381	0,09	NO
	S2	930	196	0,21	YES
	S3	272	93	0,34	YES
	S4	2419	415	0,17	YES
	S5	4024	389	0,10	YES
	S6	1073	209	0,19	YES
	S7	4937	456	0,09	YES
	S8	319	120	0,38	NO
	S9	601	95	0,16	YES
	S10	10066	1108	0,11	NO

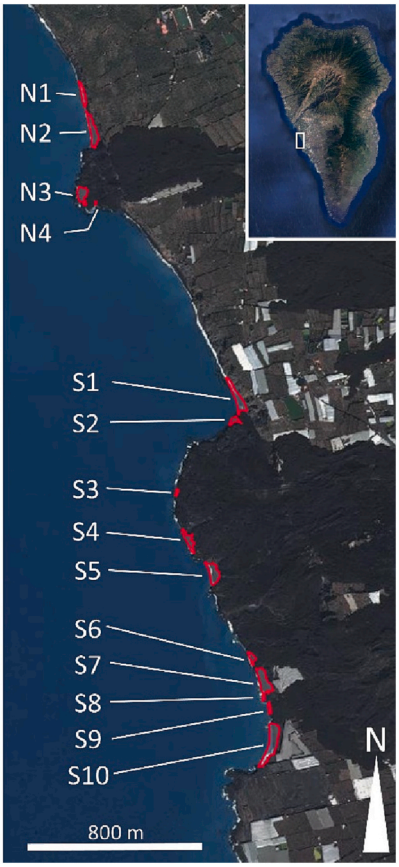

Fig. 3. Location of the different beaches whose topographic and sedimentological characteristics were measured. Shown are the beach area, the number of topographic points recorded at each site and the average density of points in each beach. The column "New beach" indicates if the beach in question is new or whether there was already a beach (though narrower and smaller) at that location before the eruption.

cross-shore beach profiles were extracted from the models. Various morphological features, including beachface slope, berm height and shoreward depressions, were obtained from the beach profiles, while alongshore topographic variations were obtained directly from the DEMs.

As for the sediment characteristics, only a few samples were collected on the beaches because most of the sedimentary material was made up of basaltic cobbles and pebbles, and only in very few places could gravel and coarse sand-sized sediments be found. For a qualitative analysis of the coarser fraction that could not be collected as hand samples, >200 vertical photographs were taken. Each one included a ruler for scale and was positioned with GPS. Visual analysis of these photographs allowed information to be obtained not only on grain size, but also on the sorting, rounding and shape of the sediment particles covering these beaches. Although different programs can be used for digital grain-size assessment from photographs (Schneider et al., 2012; Detert and Weitbrecht, 2013; Bertoni et al., 2020), it was decided not to use them as they do not give information on the rounding and shape of the particles, which is of great interest in this setting.

Submarine identification of the different geomorphological characteristics from around the front of the lava deltas down to about 40 m depth was performed by scuba divers equipped with state-of-the-art submarine photographic equipment. Though several dives were performed at different spots, it was not possible to cover the whole length of the front and flanks of both lava-deltas to make a proper submarine geomorphological cartography.

3.2. Wave data

To characterize the wave climate, SIMAR data from node 4,006,016 were obtained from the oceanographic database run by the Spanish Ports Authority. SIMAR data consist of a time series of wind and wave parameters. They are not recorded wave data, but model-derived simulations based on WAM and WaveWatch III numerical models (Puertos del Estado, 2020) with 1 datum/h. These model-derived data have been validated against recorded data showing an overall good relation (Pilar et al., 2008; Gonçalves et al., 2020). The time series used for this study covers the period 01/01/2000 to 20/05/2022. Sea level data were recorded at the La Palma tide gauge, located in the main port of the island, and the time series includes 1 recorded datum every 5 min (Fig. 1).

A storm can be defined as a wave event in which the H_s exceeds a certain threshold during a certain period of time (Mendoza et al., 2011). However, other variables are also used when modelling storminess, such as storm frequency, the inter-storm period, storm duration, the average wave height and the temporal distribution of storm significant wave heights (Dorsch et al., 2008; Harley, 2017).

In addition to the seasonal variability in wave climate, different local wave climate conditions are found in each of the Canary Islands, as well as large differences between the northern and southern coasts (Guerra-Medina and Rodríguez, 2021). For this reason, H_s thresholds for defining storm events need to be determined for each selected location.

There is a large variability in the criteria used to define a storm wave in the literature. In this work, the selected H_s threshold was based on the percentile method, which has the advantage of simplicity and robustness (Guerra-Medina and Rodríguez, 2021). Considering that it is necessary to obtain a sufficiently large number of events with an H_s threshold large enough to favor coastal reshaping, the 99th percentile of the wave data was chosen. This storm criterion aims to identify the most energetic storms with a higher potential for impact, both forming a storm berm made up of pebbles and cobbles at several meters height and contributing to the erosion of the lava delta. This is in accordance with Yanes Luque et al. (2021) whose study was also centered on the Canary Islands. The selected percentile is considerably higher than the 75th, 90th and 95th percentile used by Salvadori et al. (2020), but not as high as the 99.9th percentile chosen by Guerra-Medina and Rodríguez (2021). The use of the wave data from SIMAR node 4,006,016 covering the whole data set (01/01/2000 to 20/05/2022) ensures that the H_s threshold is related to the modal wave conditions of the site (Harley, 2017).

A minimum storm duration of 6 h was established as this is the most common criterion found in the literature (Harley, 2017). An inter-storm period of 30 h was established to separate consecutive storm events and to ensure that the different events were statistically independent (Morton et al., 1997).

Each storm was classified following the scale proposed by Mendoza et al. (2011), who define the total energy of each storm as the time integral of the squared significant wave height measured during the storm event:

$$E = \int_{t1}^{t2} H_s^2 \mathrm{d}t \tag{1}$$

where t_1 and t_2 are the beginning and the end of the storm (hours) and H_s is the significant wave height above the defined H_s threshold.

With respect to conditions associated to swell dominance, these are important because berm build-up has been reported under high wave period values and low wave steepness values ($H/L < 0.01$), while situations characterized by low wave periods and relatively high steepness ($H/L > 0.01$) are representative of wind-wave conditions, during which berm erosion is expected to occur (Komar, 1998; Masselink et al., 2010).

The two contrasting situations are separated by steepness values smaller or higher than 0.01. To avoid the uncertain pattern of situations in which $H/L \approx 0.01$, both opposite situations were separated by a region in which sediment transport could be considered in balance between the upward and backward directions. This region is defined by low energy waves (those under the defined threshold of storms waves) with intermediate steepness values ($0.008 \leq H/L \leq 0.012$).

3.3. Morphologic and morphodynamic parameters

The morphodynamic parameters relate morphological characteristics with wave climate (Casamayor et al., 2022). Beachface slope and run-up are the parameters chosen to characterize beach morphodynamics.

In general, the most widely used morphological variable is the beachface slope. There is some variation in the scientific literature regarding how the term is applied (McGlashan et al., 2005), but most researchers agree that the beachface is the area between the low tide mark and the upper limit of high-tide wave run-up (Jennings and Shulmeister, 2002; Masselink and Li, 2001; Reis and Gama, 2010; Bujan et al., 2019). If there is a berm, the upper limit of the beachface is the berm crest.

Several profiles were extracted from the 2022 DEM for all beaches and used to measure the beachface slope ($\tan\beta$). Spatial separation between profiles was 20 m, except for the smaller beaches where the profiles were spaced approximately 17 m apart from each other.

Following the previously mentioned definition, the beachface slope was calculated considering the distance between the crest of the tidal berm and the mean low water (MLW = − 0.5 m), and the elevation difference between the two points. In cases when the 2022 DEM did not reach the MLW level, the seawardmost part of the profile was used.

Run-up is one of the most important morphodynamic parameter in gravel beaches, since it is related with onshore sediment transport and berm formation (Horn and Li, 2006; Pedrozo-Acuña et al., 2006). While different expressions can be used to compute wave run-up, this work calculates the 2% exceedance run-up using two equations developed by Poate et al. (2016). Both equations are suitable for coarse grain beaches, since they are based on data collected from beaches whose grain size ranges from gravel to pebble. They are very similar, with the only differences being the variable used for the wave period and the empirical coefficient.

$$R_1 = 0.33 tan\beta^{0.5}\ T_P\ H_s \quad (2)$$

$$R_2 = 0.49 tan\beta^{0.5}\ T_z\ H_s \quad (3)$$

where tanβ is beachface slope, T_p is peak wave period, T_z is mean wave period and H_s is significant wave height.

Both equations were applied in two different ways: With the first, the aim is to obtain the average run-up and it is obtained from the average values of the wave-derived variables (T_p, T_z and H_s) without considering sea level data. These run-up values are expressed as $R_{1,av}$ and $R_{2,av}$. The second way involves computing the run-up values that are only exceeded by 2% of the waves. In this case, associated sea level variations were considered denoted by $R_{1,2\%}$ and $R_{2,2\%}$. In both cases, the wave data series was restricted to the period between the initial stages of lava delta formation (29 September 2021) and the collection of data for this study (9 May 2022).

The submarine part of the beach profile where most cross-shore transport takes place is the upper shoreface, and its seaward limit is defined by the depth of closure (D_c). It corresponds to the most landward depth seaward of which there is no significant change in bottom elevation during a given time interval (Kraus et al., 1998). There are several formulas to estimate the closure depth. Of these, the Hallermeier (1981) equation was used in this work:

$$D_c = 2.28\ H_{sx} - \frac{68.5\ H_{sx}^2}{gT_e^2} \quad (4)$$

where H_{sx} is the storm wave height that is only exceeded 12 h/y, T_e is the associated wave period and g is gravity acceleration. The time interval was also restricted to the period 29/09/2021–9/5/2022.

3.4. Estimation of the volume of materials in the beaches

As some beaches already existed before the Tajogaite eruption and others were newly formed (Fig. 3), two different approaches had to be used to estimate the volume change of sedimentary material.

For beaches that already existed before the eruption, the volume of accumulated/eroded material was computed after comparing the DEM measured in this study, hereinafter named 2022 DEM, and a previous DEM obtained from LiDAR data collected in 2020 with a maximum uncertainty <0.20 m (GRAFCAN, Canary Islands Government) named 2020 DEM. In most cases, the amount of material accumulated because of the eruption determined that the shoreline in the 2022 DEM was more seaward than it was in the 2020 DEM when the beaches were much narrower. To obtain a better approximation of the total volume of sediments accumulated after the eruption, both DEMs had to be enlarged towards the ocean. The submerged part of the profile prior to the eruption was obtained from bathymetry performed in 2003 within the framework of the ecocartographic study of the La Palma shoreline, available at https://www.opendatalapalma.es/documents/ecocartografico/about, whose maximum uncertainty is <0.25 m. The submarine part of the 2022 DEM was extrapolated assuming a constant slope equal to the one measured in the most seaward meter in the 2022 DEM. This part was extended untill it reached the 2003 bathymetry (Fig. 4A).

The newly formed beaches after did not exist at all before the Tajogaite eruption, since they are located in areas where the previous bathymetry was between 5 and 15 m depth. Therefore, it is not easy to provide a comparison with a situation prior to the 2022 DEM. Nevertheless, a DEM obtained from a photogrammetric flight performed in December 2021, a few days after the end of the eruption, was used. The RMS reprojection error of this DEM is 0.144 m. This DEM (hereinafter named 2021 DEM) shows the lava delta recently formed, with a highly irregular topography typical of active volcanic settings. In many places the lava flows feeding the lava deltas end in sharp cliffs several meters high, while in other locations there are small beach-like deposits. The 2021 DEM was compared to the 2022 DEM. In most cases, beaches in the 2021 DEM were narrower than in the 2022 DEM. The 2021 DEM was therefore extended seawards to reach the same length as in the 2022

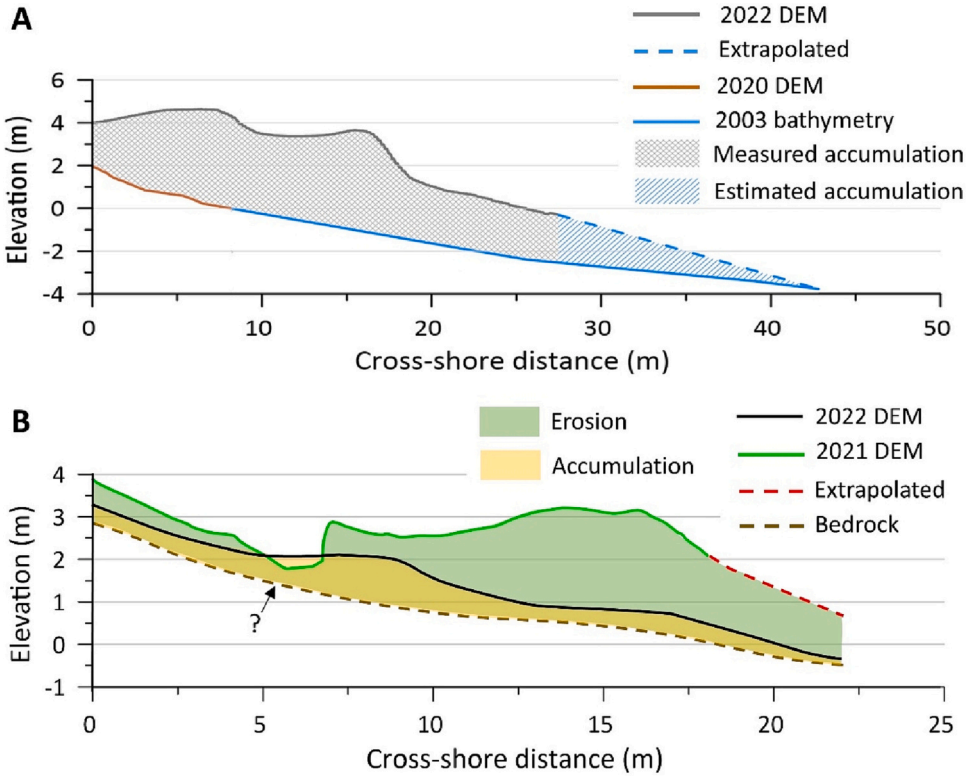

Fig. 4. Schematic representation of the methodology and the different data sources used to compute the volume change in the previously existing beaches (profile N2–5, A) and the newly formed ones (profile S4–2, B). Note in B that the bedrock profile has not been measured but estimated.

DEM by extrapolating the shallowest part of a bathymetric study carried out in May 2022 when the lava deltas already existed. This bathymetry is available at hppt://visor.grafcan.es. In this case, the two DEMs do not end at the same depth (Fig. 4B).

In most cases the measured topography in the 2022 DEM was at a lower elevation compared to the 2021 DEM indicating that the lava flow had been eroded. Considering that these new beaches are formed from the later accumulation of these eroded materials, a bedrock surface was assumed to be between 0.4 and 1 m below the measured topographic data. Therefore, for these beaches the volume of accumulated sediments was computed by multiplying the beach area by an average thickness of the sedimentary layer of 0.7 m.

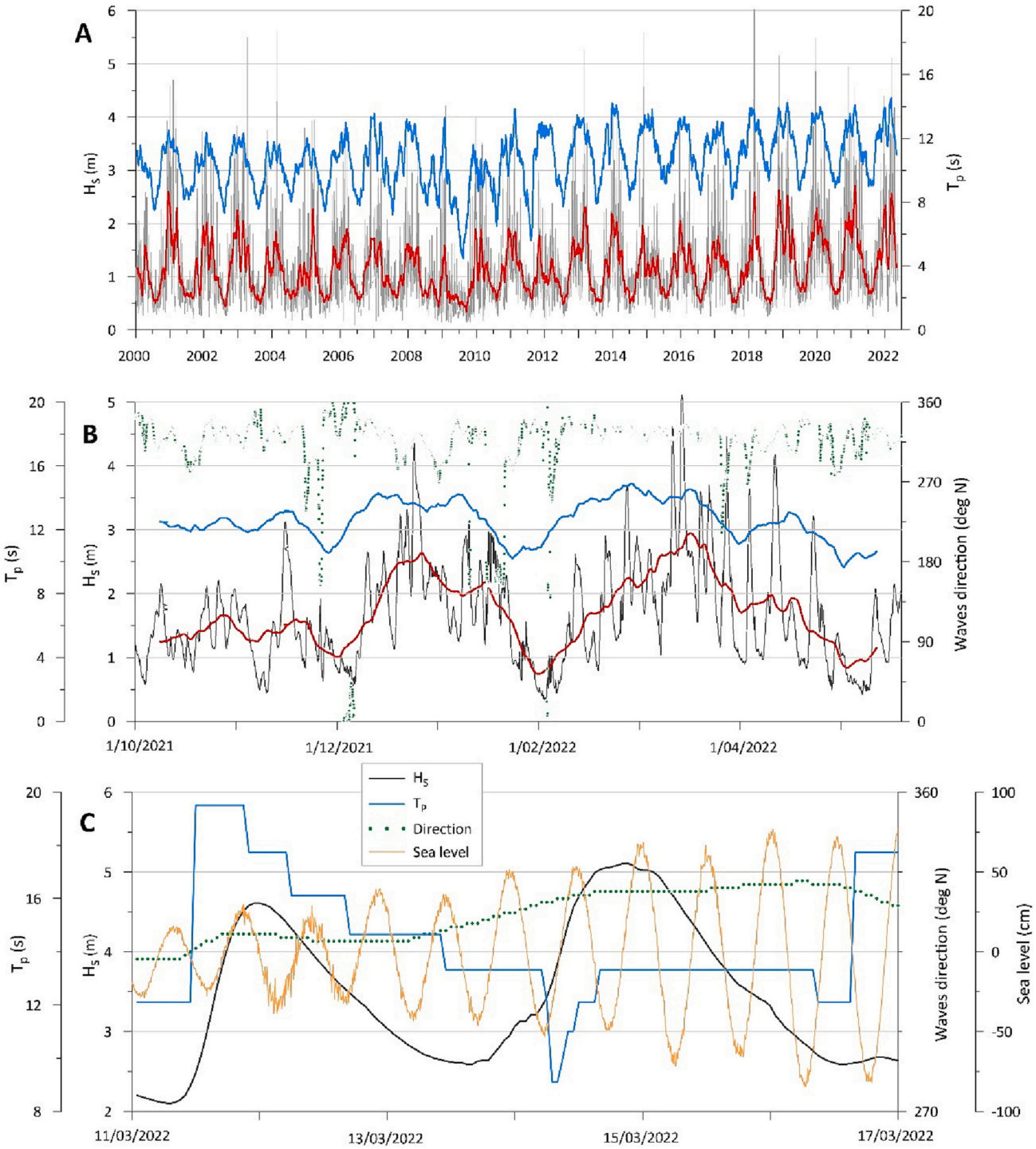

Fig. 5. A) Hourly wave data from SIMAR node 4,006,016 from 01/01/2000 to 15/05/2022, showing the seasonal pattern of H_s (grey lines) and T_p. Red and blue lines represent the moving average of H_s and T_p respectively, with a window of 729 data corresponding to 1 month. B) Hourly time series from SIMAR node 4,006,016 of H_s, T_p and wave direction during the 2021/2022 autumn-winter season. The moving average of H_s and T_p (red and blue lines, respectively) has a window of 363 data corresponding to 15 days. C) Idem for days 11–16 March 2022, when the two most severe storm events took place. 5-min sea level data recorded at Santa Cruz de La Palma harbor are also shown.

4. Results

4.1. Wave climate

Wave climate in the study area follows a clear seasonal pattern, with much higher and longer waves in autumn-winter compared to those occurring in spring-summer (Fig. 5A). The autumn-winter season of 2021–2022 showed an extraordinary number of events of high waves. Up to 14 energy events with $H_s > 3$ m were recorded from November 2021 to April 2022, with 5 of them having $H_s > 4$ m. In all these events, the mean wave direction was W-NNW, revealing a fetch of several thousand kilometers (Fig. 5B). Based on the statistical approach of the 99th percentile, storms were defined by an H_s threshold of 3.48 m.

Two different wave conditions have been reported as responsible for onshore transport and potential storm berm build-up. One of them is related to high energy waves, normally linked to storm events, and the other one is associated to large swell situations with low wave steepness values ($H/L < 0.01$).

During the period between the initial stage of formation of the first lava delta (29 September 2021) and the conclusion of data collection for this study (9 May 2022), up to nine storms were recorded in the area, all of them exceeding the defined criteria for wave height threshold, storm duration and inter-storm period (Table 1). According to the five-grade scale proposed by Mendoza et al. (2011), where class I is the weakest and class V the most severe, two of the storms corresponded to class IV (severe storms), two to class III (moderate) and five to class I (weak). Fair weather conditions between consecutive storms lasted two months between storms 1 and 2, and just a few days between the other storms.

Most of these high energy events lasted sufficiently long for part of them to take place at high tide. This is the case of the strongest storm event, which took place during days 14 and 15 of March 2022 (Fig. 5C). Storm waves ($H_s = 5.1$ m, $T_p = 12.5$ s) from the NNW hit the western coastline of La Palma over the course of 38 h. This happened close to the spring tides, which strengthened the wave attack on the shore. The resulting D_c value derived after applying the Hallermeier (1981) equation is 10.3 m.

The combined effect of wave storms and wave steepness allows to define 4 different regions regarding berm formation/destruction (Fig. 6). The high energy waves are those when $H_s > H_s$ threshold (region A), and for the low energy waves there are three possible regions according to their wave steepness values: $H/L < 0.008$; $0.008 \leq H/L \leq 0.012$ and $H/L > 0.012$ (regions B, C, and D, respectively).

The relative importance of these four regions is shown for two wave data series (Table 2). One (lasting from 01/01/2000 to 20/05/2022) is representative of dominant wave conditions in the study area, while the second only covers the formation period of these beaches (29/09/2021–09/05/2022). In both cases the storm threshold defined by $H_s > 3.48$ m is considered a primary condition, so that storm data are not classified according to their wave steepness value (Fig. 6).

4.2. Beach morphology

Thirteen gravel beaches were formed along the coastal front of the two lava deltas, including newly formed beaches and others that were substantially modified after the Tajogaite eruption. The high irregularity of the lava delta front mostly favored the development of these gravel accumulations at small headland-embayment beaches between lava flows, but they can also be found along certain points of the lava front or attached to the northern and southern extremes of the lava deltas (Fig. 7).

4.2.1. Digital elevation models (DEMs) and profiles

Detailed topographic measurements were taken in all the beaches and the resulting DEMs were developed (Figs. 8, 9 and 10). The plan view of some of these beaches is rather irregular due to the presence of the surrounding lava flows that encapsulate them (e.g. beaches N3, S2 and S4). Some of the beaches show a fully developed profile, while others are much smaller and/or narrower since they are bounded either by lava flows (beaches N4, S2, S3, S6, S8 and S9) or by the back cliff (beaches N1 and northern part of S1).

In general, these gravel deposits are highly irregular, showing abrupt morphological changes both across and along the coastline. The smaller beaches present smooth slopes (beaches N4, S3, S8 and S9), while the larger beaches present strong irregularities, both in the foreshore (beaches N2, S1, S6, S10) and backshore (beaches N3, S5, S6, S7, S10). Foreshore irregularities are mostly related to the presence of berms and beach cusps, while those on the backshore are described in subsection 4.2.3 (Fig. 11).

All the DEMs used to calculate the volume changes are shown within the Supplementary Material part 1, while all the cross-shore beach profiles, including its submerged portion, used to calculate the beachface slope in the different beaches are included in the Supplementary Material part 2.

4.2.2. Beach morphological features and run-up

Beaches under study present large differences both in size (area, length of the coastline and average width) and elevation (maximum and average height), with all these morphological features derived from the DEMs (Table 3). N4 beach is the smallest (just 88 m^2 in size and 6.6 m of coastline) and S10 is the largest beach (over 10,000 m^2 in size and with a coastline length of 222 m. Beach elevation is considerable, particularly considering that most of the beaches are quite narrow. The average height of all the topographic points measured above 0.5 m is 3 m or above in five beaches, and the maximum height is 5 m or above in eight beaches (Table 3).

The beachface in most beaches is very steep, with values ranging between 0.11 and 0.57 for individual beach profiles (Fig. 11). Considering the average beachface slope when several beach profiles were measured at one beach, the steepest beaches are N2 and S1, with slopes higher than 0.3, while the lowest slope values are found in beaches S9, S4 and N4 (Table 3).

Table 1
Main characteristics of the nine storms that took place between the beginning of the lava delta formation and the conclusion of data collection for this study. H_{max} is the maximum recorded value of H_s. H_s, T_p and Dir refer to the average values of these wave properties during each storm. E is total energy. Storm class is derived from the Mendoza et al. (2011) scale. Tide indicates the highest recorded elevation above mean sea level.

Event	Start date/h	Duration (h)	H_{max} (m)	H_s (m)	T_p (s)	Dir (°N)	E (m^2h)	Storm class	Tide (cm)
1	23/12/2021 17:00	48	4.4	3.8 ± 0.3	16.0 ± 1.1	322 ± 2	710	IV	75
2	25/02/2022 23:00	14	3.7	3.6 ± 0.1	18.0 ± 1.1	335.4 ± 0.5	183	I	50
3	11/03/2022 16:00	26	4.6	4.1 ± 0.4	17.3 ± 1.5	319.1 ± 0.9	446	III	30
4	14/03/2022 07:00	38	5.1	4.5 ± 0.6	12.8 ± 1.2	331.9 ± 1.0	776	IV	69
5	20/03/2022 07:00	11	3.6	3.6 ± 0.0	15.2 ± 0.7	317.1 ± 1.7	139	I	104
6	22/03/2022 23:00	7	3.7	3.6 ± 0.1	16.1 ± 0.0	321.4 ± 0.5	90	I	80
7	28/03/2022 04:00	12	4.5	3.9 ± 0.3	13.3 ± 0.0	273.5 ± 6.2	186	I	74
8	04/04/2022 00:00	9	3.6	3.6 ± 0.0	12.0 ± 0.4	285.9 ± 4.2	116	I	101
9	11/04/2022 10:00	30	4.9	3.9 ± 0.2	15.3 ± 0.7	332.5 ± 3.2	465	III	54

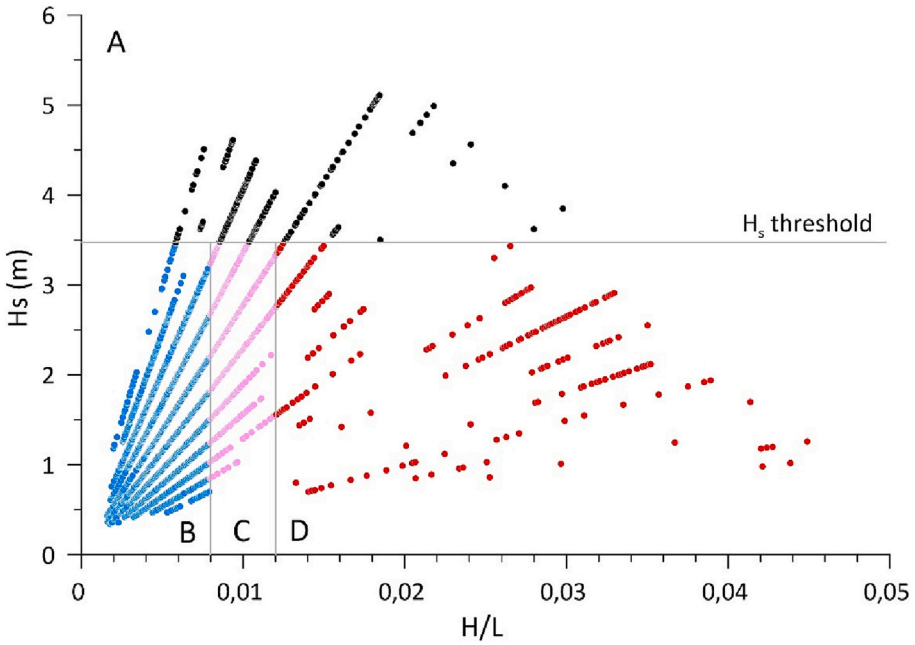

Fig. 6. Diagram showing the four different regions (A, B, C and D) in which wave conditions can contribute to berm construction, maintenance or destruction (see text). Plotted wave data correspond to the seven-month period between the beginning of the formation of the lava deltas and the collection of data for this study.

Table 2
Classification of wave data in the four regions defined in the text and Fig. 6, both for the modal wave climate and for the period when the beaches under study were formed.

Region		A	B	C	D
Dominant process		Onshore transport / berm build-up		Equilibrium	Berm erosion
	N° Data	H_s > threshold	H/L < 0.008	0.008 ≤ H/L ≤ 0.012	H/L > 0.012
Modal conditions	193780	1967	13112	47345	131356
		1%	6.8%	24.4%	67.8%
Beaches formation	5296	195	3931	926	244
		3.7%	74,2%	17,5%	4,6%

Morphological irregularities, with consecutive highs and lows along the shoreline are a common feature in all the studied beaches, including at the N1 beach which is considered outside the influence of the lava deltas (Figs. 7A, 12). This example shows two alongshore profiles derived from the corresponding DEMs along the foreshore at the N2 and S1 beaches. Even though there is no regular pattern, in both cases the height differences and spacing resemble a cusp-like morphology, with a distance between consecutive horns of around 10 m.

Berm morphologies are present in most of these beaches. In the wider beaches where the profiles are fully developed, two berms can be found. The lower one is the so-called tidal berm, which is normally found between 2 and 3 m above mean sea level, while the upper one is the storm berm, located at 4–5 m height. The only exceptions are the N1, N4 and S9 beaches (Fig. 11, Table 3), where no berm is present.

The average run-up values obtained using the Poate et al. (2016) equations are around 0.4 m higher when using T_p instead of T_z (Eqs. (2) and (3), respectively), while $R_{2\%}$ values follow the opposite pattern, with the values derived after T_z 0.3 m higher than those obtained with T_p. Despite these differences, the average run-up values are higher than the maximum beach elevation at the S3, S8 and S9 beaches, while $R_{2\%}$ values are considerably higher than the maximum beach elevation at all the beaches (Table 3).

4.2.3. Backshore

In most cases, the backshore is generally more uniform than the beachface, though in certain cases it is also highly irregular, with abrupt topographic changes observed on the backshore of the N3 and S5 beaches. Apart from these topographic irregularities, three other aspects should be highlighted. The first is the presence of wood debris on the wider beaches (Fig. 13). This debris mostly consisted of tree branches, canes and some pine cones. They were found in the longshore direction at some distance from the shoreline, along the upper part of the gravelly deposits shoreward of the storm berm. The topographic elevation of the debris ranges from 4 to 6 m above mean sea level in the different beaches.

The second point of interest is the lower elevations observed in the most landward part of the wider beaches. This morphological depression can be identified in the N2, N3, S2, S5 and S10 beaches, as well as in the southern part of S1 and the northern part of S7. These topographic lows seem to indicate that the accumulation of gravelly deposits does not reach the inner limit of the broader beaches.

The final point of interest to highlight is the presence of well-rounded boulders, which are the result of wave action over a long period of time. These boulders were only found at two places: alongside the cliff in the SE corner of beach S1 (Fig. 13E), and along the landward limit of beach S10 (Fig. 13F). These boulders are remnants of the beaches that existed in those areas before the eruption and the formation of the actual beaches, but which today are >40 m from the shoreline.

4.3. Beach volume

The volume of sediments accumulated on the beaches is estimated to

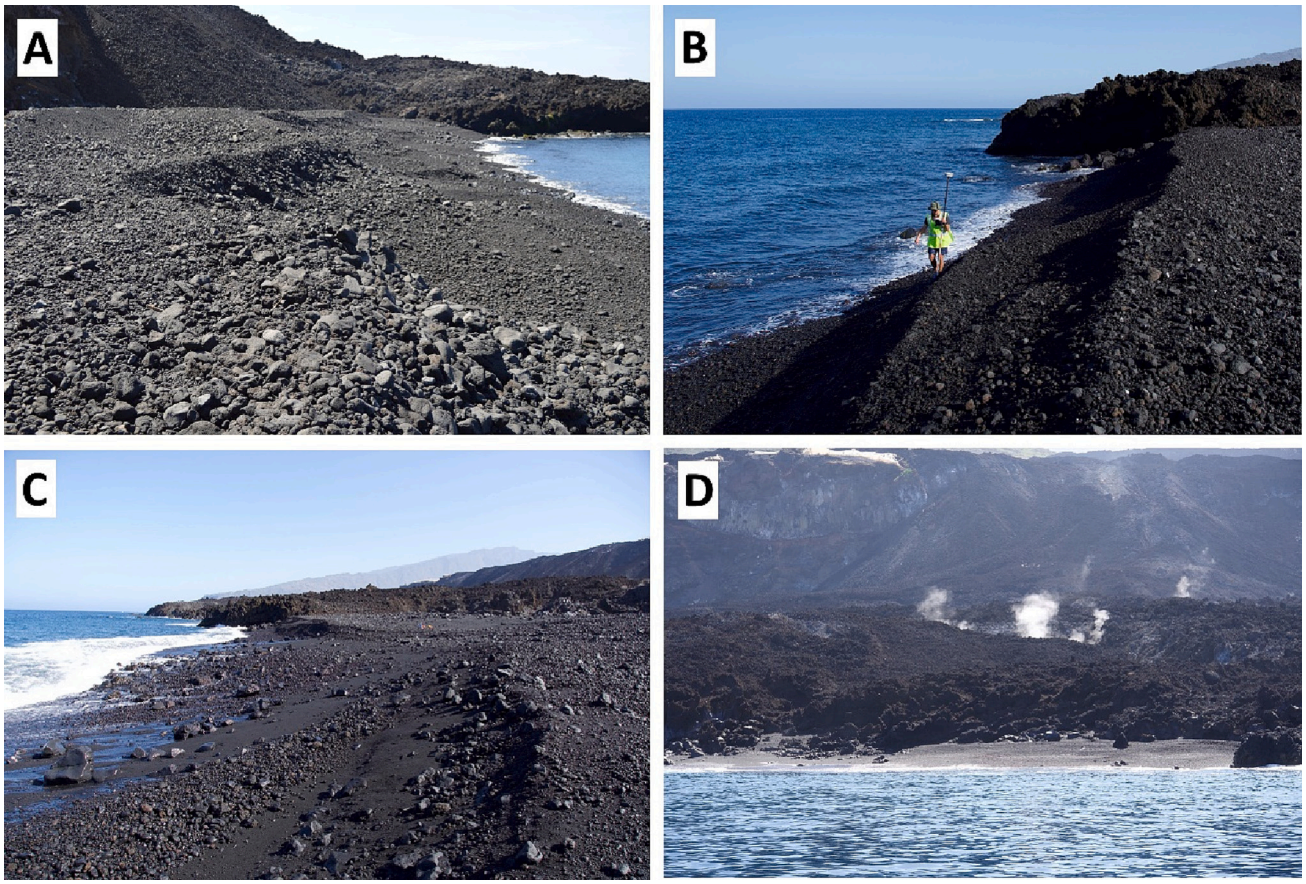

Fig. 7. General photographs of some of the beaches under study. A) Beach S1, attached to the cliff and bounded by a lava flow at the southern end. Note the irregularity of cusp-like morphologies along the coastline. B) Beach S7, located between two lava flows. Note the high steepness of the foreshore and the double berm. C) Northern part of S10 beach. Note the diversity of sediment size, ranging from coarse sand to boulders. D) Frontal view of S6 beach. Note the gas emissions some meters inland.

be around 79,000 m^3, with 16,200 m^3 corresponding to the beaches associated to the northern lava delta and 62,800 m^3 to those associated to the southern one (Table 4). Approximately 69% of this amount was directly measured after comparing the different DEMs used, while the remaining 31% was estimated (Fig. 4). The beaches that already existed before the eruption (those indicated by N in Table 4) present a net sediment accumulation of 67.000 m^3, while the newly formed beaches (indicated by Y in Table 4) give an estimated volume of 12.000 m^3.

4.4. Sediment characteristics and submarine features

Sediment composition is highly uniform, with 100% basaltic material found in all the beaches. However, its textural properties show important variations. Grain size ranges from coarse sand to boulders, sorting varies locally from well-sorted near-uniform size classes to poorly sorted mixtures of different clasts, while particle roundness fluctuates between well-rounded to very angular.

These changes can be identified both alongshore and cross-shore. Along the foreshore, sediment size can range from coarse sand to boulders within a few meters (Fig. 7C), but these changes in sediment texture are more marked in the cross-shore direction. In most beaches, the foreshore is made up of well-sorted subrounded pebbles and cobbles, though some coarse sand and gravel patches are also present, normally associated to topographic lows or sheltered areas (Fig. 14A, B, C). The berm tends to be composed of near-uniform subrounded pebbles and cobbles. In contrast, the backshore is made up of a poorly sorted mixture of materials ranging from gravels to cobbles. Their shape is much more angular, with sharp edges, which indicates that abrasion due to wave action has not taken place. Packing in this area is very low (Fig. 14D, E, F).

There are two main geomorphological features found in the submarine part of both lava deltas: pahoehoe-type lava flows and large accumulations of coarse-grained volcanoclastic fragments. The surface of the submerged lava flows is made up of highly vesicular scoriaceous materials (Fig. 15A). Present in these lava flows are submarine pillow structures, rocky arcs and brecciated volcanic megablocks several meters high are present (Fig. 15B). Where these elements are located at low depths, they are continuously being dismantled due to wave action.

As for the extensive deposits of volcanic fragments, they are found covering large areas from about 5 to 25 m depth and are found laterally resting on the sandy bottom of the inner shelf (Fig. 15C, D). These accumulations are poorly sorted since they are mostly composed of loose decimetric-sized pieces of volcanic scoria alternating with metric-sized volcanic blocks. Clasts show irregular forms and their edges are slightly rounded as a result of rolling due to wave action. Average size ranges from coarse pebbles to fine cobbles ($16 < D_{50} \leq 128$ mm, Fig. 15F).

5. Discussion

5.1. Volume of sediments and beach patterns

Different DEMs were compared for all beaches in order to obtain the volume of sediments accumulated on the beaches under study. Two different approaches and data sources were used depending on whether the beach already existed or was newly formed (Fig. 4). Overall, it was

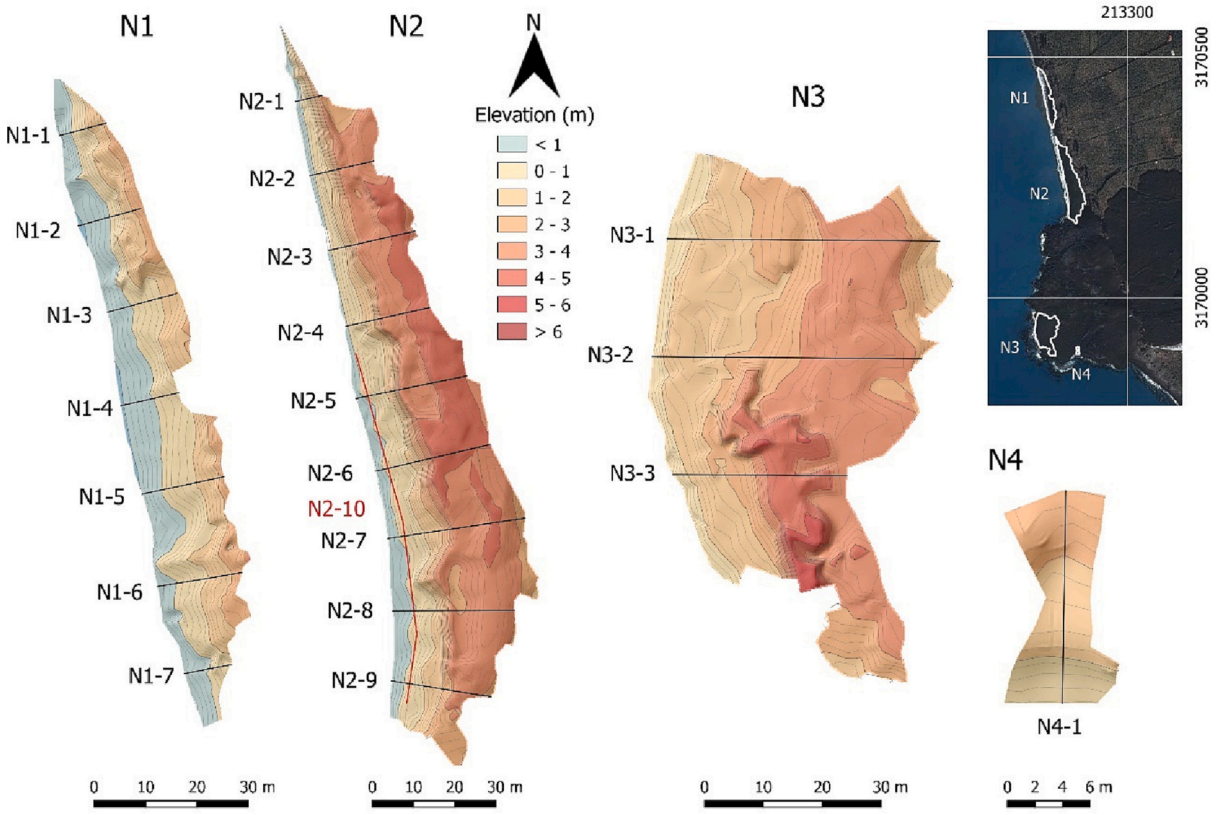

Fig. 8. Digital elevation models of beaches N1-N4 associated to the northern lava delta, with the corresponding cross-shore (black) and longshore (red) profiles. Elevation corresponds to the officially defined mean sea level for La Palma Island.

found that a total of 79,000 m^3 of sediments had accumulated on the different beaches formed along the two lava deltas.

Despite this net accumulation, it should be noted that different patterns were found in previously existing beaches compared to newly formed ones. In the first group, all beaches showed high accumulation values, with the exception of beach N1. This beach can be considered as the only natural unaltered beach and is deemed to be a benchmark as it was not affected by the 2021 eruption and the subsequent formation of the lava deltas. Considering its dimensions (1658 m^2, Table 3), the obtained volume change (−107 m^3, Table 4) gives an area-normalized volume on −0.06 m^3/m^2, indicating that this beach is very stable, as would be expected for a narrow beach attached to the cliff toe. The other beaches in this group (namely N2, S1, S8 and S10 beaches) significantly increased their volume by >67,000 m^3, resulting in a net increment in beach amplitude and height. The area-normalized volume gives values higher than 2.5 m^3/m^2 y three of these beaches (Table 4), indicating that the average thickness of sediment accretion is very big. The stability of beach N1 lies in contrast with the considerably large amount of sediments accumulated on the rest of the beaches and highlights that the closer to the lava deltas the higher the amount of sedimentary material available for accumulation on the beaches.

With respect to the beaches formed after the eruption, they present an accumulation of about 12,000 m^3. In these beaches, the DEM corresponding to the previous situation was derived from a photogrammetric flight obtained just a few days after the end of the eruption and, in many locations, represents the abrupt and irregular surface of the lava flows. The fast erosion of these volcanic materials can be attributed to two major conditions: (*i*) the well-known fragility of volcanic scoria, and (*ii*) the high energy waves that hit this area (Fig. 16). It can be expected that most of the eroded materials accumulated on the submerged part of the lava delta within the first few meters to the shoreline were then transported onshore, giving rise to the formation of these new beaches. Therefore, the higher the sequence of storms the greater the lava front erosion and the higher the number of sediments available to form these beaches. The average thickness of the beach deposit was estimated at around 0.7 m, which is quite conservative considering that most berms are >1.5 m high from the base to the top.

5.2. Sediment sources

The development of gravel beaches requires an abundant supply of gravel-sized particles. This material normally originates from sediments eroded from mountains or cliffs or transported by rivers and glaciers (Pontee et al., 2004; Shulmeister and Kirk, 1997). Different sediment sources could be responsible for the formation of the narrow beaches that can be found at the base of the cliff along the western coast of La Palma: *i*) cliff rockfalls, which are quite common due to cliff verticality and can be easily observed from offshore (Fig. 2B); *ii*) fluvial runoff (mainly but not only from Barranco de Las Angustias). These materials could subsequently have been distributed along the coastline by longshore drift; *iii*) coastal erosion due to high energy waves; *iv*) aerial deposition of volcanic ash and pyroclasts, as well as materials produced from wave abrasion of lava flows following its contact with seawater, directly related to volcanic eruptions; and *v*) the island shelf, in which case sediments could be pulled up to the coast by onshore transport. The first four sources imply exclusively sediments of terrigenous provenance (clasts and grains derived from volcanic origin), while shelf materials could be either terrigenous or bioclastic. Regardless of the origin, sediments on these beaches range from sand to cobbles and are mostly rounded due to continuous wave action (Carracedo et al., 2001; Calvet et al., 2003; Marrero et al., 2017).

The formation of the new beaches under study is related to the arrival of about 79,000 m^3 of gravel in less than seven months. Cliff rockfalls cannot explain this amount of new material, since some of the

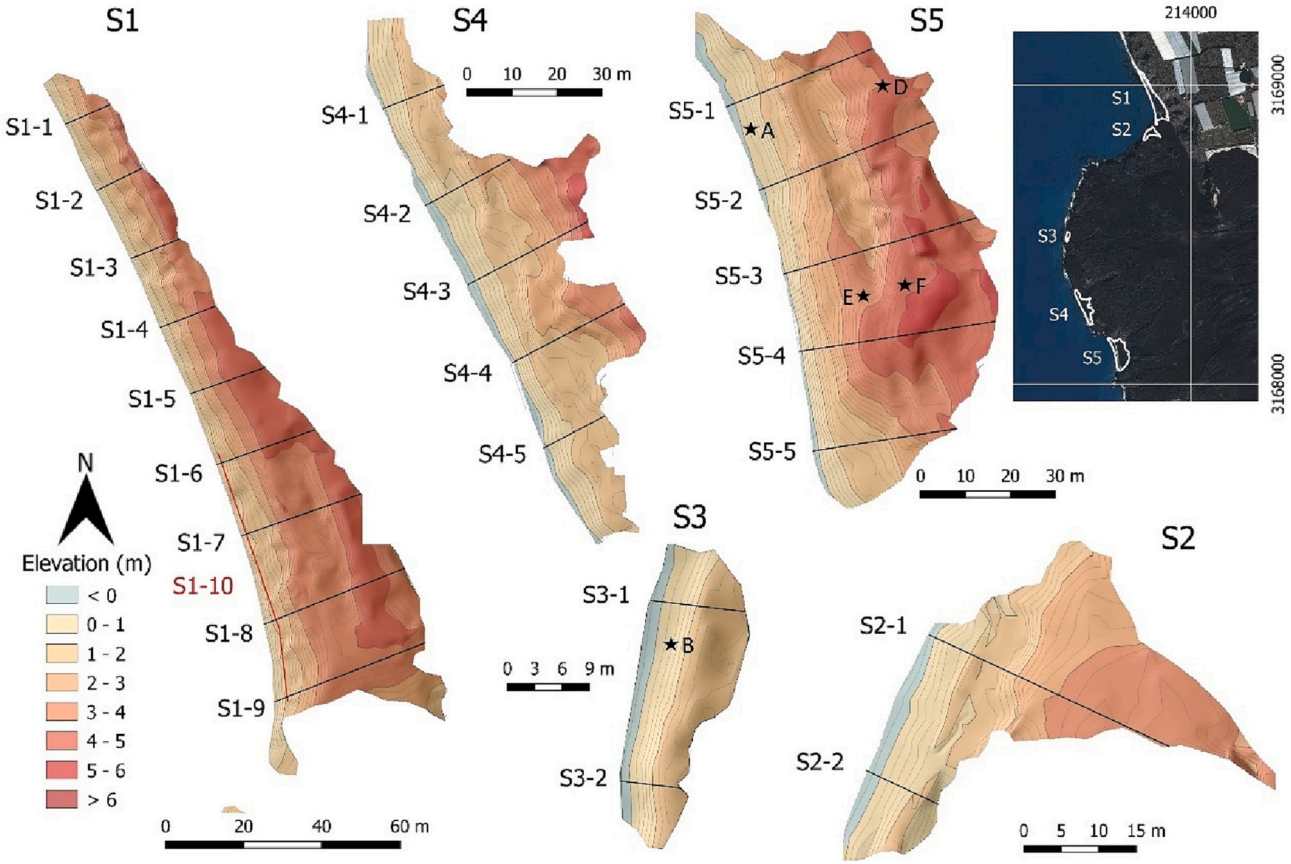

Fig. 9. Digital elevation models of beaches S1-S5 associated to the southern lava delta, with the corresponding cross-shore (black) and longshore (red) profiles. Elevation corresponds to the officially defined mean sea level for La Palma Island. Black stars correspond to the images shown in Fig. 14.

beaches are located on the front of the lava deltas, far from the cliffs. Fluvial discharge through Barranco de Las Angustias was negligible during the 2021–2022 winter, while longshore drift may eventually have contributed to the formation of sedimentary deposits attached to the north flank of the deltas but never along the front or southern flanks. Volcanic ash does not have the dominant size of beach particles and has only been found in the inland areas of the largest beach, beyond the reach of wave action (Fig. 13Fb). Therefore, the only possible source areas that could explain the formation of these beaches are the erosion of the lava delta front and the onshore transport of the scoria fragments located underwater. This is in agreement with Calvet et al. (2003) who report that although marine erosion is a continuous process the period of major sediment input towards beaches is probably related to volcanic eruptions. Romagnoli et al. (2006) also argue that beach accretion at Stromboli occurred during/after major eruptive crises when subaerial lava flows entered the sea.

The lava delta front is formed either by compact and dense lava flows or by highly irregular and vesiculated volcanic scoria. The hardness of the two types of volcanic material differs considerably as the lavas are much harder than the scoria fragments. Areas mostly covered by these brecciated materials are intensively fragmented and disintegrated into smaller pieces due to wave action. This is the reason why the 2021 DEM is generally at higher elevation than the 2022 DEM (Fig. 4B).

The erosion of these volcanic material is a key source of materials that contribute to forming the new beaches. As stated by Leont'yev (2022), there is a relationship between the volume of erosion at the delta front and the volume of the growing beach. Nevertheless, the erosion of the lava deltas front cannot explain by itself the accumulation of 79,000 m^3 of sediments, mostly in only four beaches (Table 4).

5.3. Onshore transport and berm formation

The huge accumulations of scoria fragments located in the submarine portion of the lava delta (Fig. 15C, D) could have been transported shoreward and contributed to forming the accumulations of clasts identified on the beaches. The only transport limitations for these clasts are particle size and density, depth, and the existence of waves capable of moving them.

These submarine volcanic clasts were classified through visual analysis of the underwater photographs as coarse pebbles to fine cobbles ($16 < D_{50} \leq 128$ mm, Fig. 15D). This size could be initially considered a limitation for transport, but these scoria fragments are highly vesiculated, and therefore their specific gravity is much lower than the equivalent for more compact particles of the same size. Additionally, their irregular shape favors intraclast porosity and subsequent sediment entrainment by waves. In fact, scoria clasts from Tajogaite eruption were studied by Romero et al. (2022), who determined that its vesicularity ranges from 58 to 79 vol%, yielding particle densities between 1881 and 2152 kg/m^3. These density values are much lower than the average density of the siliceous materials (2650 kg/m^3) normally found in sediment transport formulations.

This is in agreement with Richmond et al. (2011), who showed how the effect of storm waves combined with minor tectonic uplift was capable of building a significant ridge complex thanks to the arrival of nearshore basalt boulders in <30 years. Voropayev et al. (1998) measured the movement of cobble-sized particles in a wave-induced oscillatory flow under laboratory conditions, while Brayne et al. (2020) assessed the entrainment of cobbles by waves in field conditions. These authors measured the movement of 14 cobbles deployed in the nearshore zone during a series of five discrete storm events ($0.10\ m < H_s < 0.52\ m$) at Flathead Lake, Montana (USA), finding the entrainment

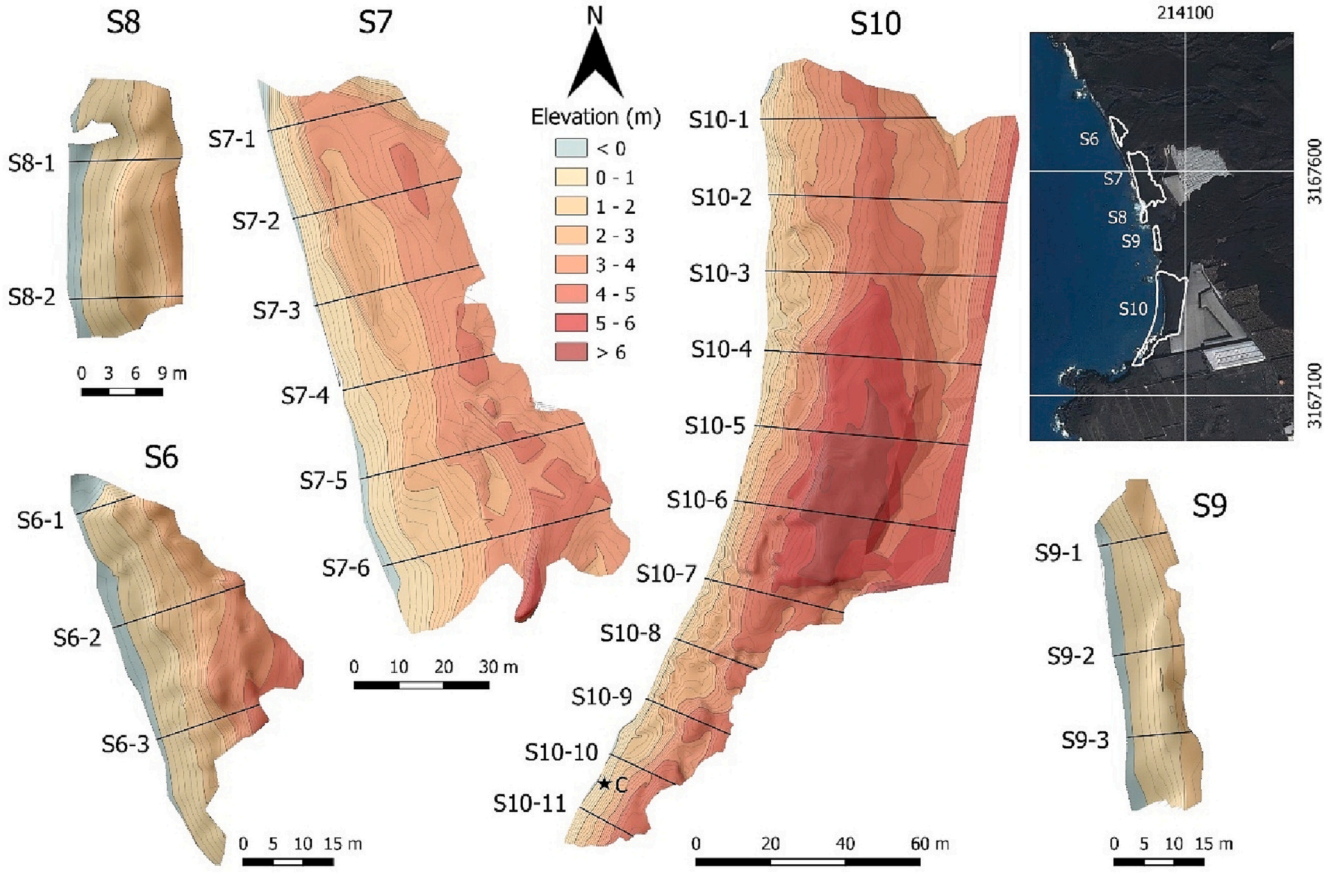

Fig. 10. Digital elevation models of beaches S6-S10 associated to the southern lava delta. The location of the different cross-shore profiles within each beach is also shown. Elevation corresponds to the officially defined mean sea level for La Palma Island. Black stars correspond to the images shown in Fig. 14.

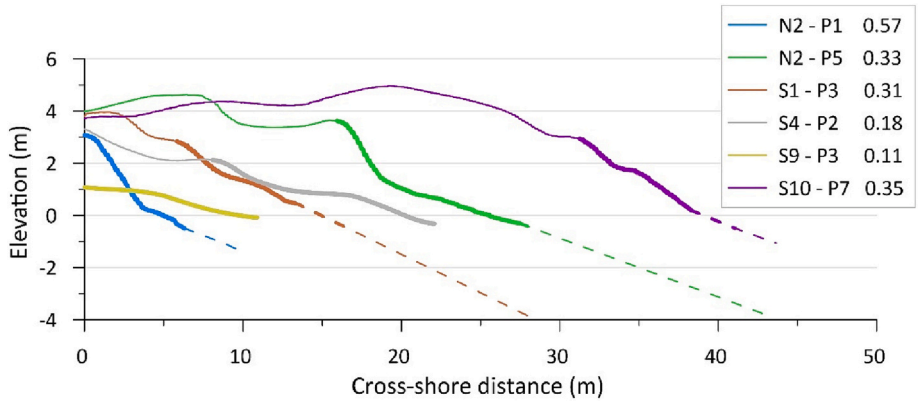

Fig. 11. Selected cross-shore beach profiles from the beaches shown in Figs. 8, 9 and 10, including those with the highest (N2-P1) and lowest (S9-P3) beachface slope values. The dashed line is the extrapolated portion of the profile. The section in bold is the one used to calculate the beachface slope, which is shown in the legend. Note that where the profile is wide enough, it normally shows two berms.

threshold to be positively related to wave power. The wave energy conditions recorded at La Palma Island are much higher than those reported at Flathead Lake, and therefore the size of the volcanic clasts would not be a problem for their movement.

The depth of closure of 10.3 m obtained after applying the Hallermeier (1981) expression might be considered the limit of significant cross-shore transport, so that any particles located landward of the depth of closure might be pulled up to the swash zone and eventually to the berm by waves. Masselink et al. (2010), based on experimental data, suggested that onshore swash zone sediment transport is heavily affected by the advection of sediment entrained at the wave breakpoint into the swash zone during the uprush. Pedrozo-Acuña et al. (2006), based on large-scale experiments, concluded that most of the profile change on gravel beaches occurs across the swash zone, with the area below the sea water level being eroded while the berm is developed. Bertoni et al. (2010) demonstrated that coarse-grained particles could move either from the submerged part of the beach to the subaerial part or vice-versa. Though none of these works relate the moving particles to the depth of closure, both large-scale tests and field experiments have shown that coarse-grained sediments can be pulled up from the submerged part of the beach profile at several meters depth to the swash zone, and from there to the berm. The only limitation would be the type

Table 3
Main features obtained for the different beaches. Length was measured along the coastline. Average Width was obtained after dividing Area by Length. Average Height was obtained from measured elevation of all topographic points located above 0.5 m to avoid tidal differences when surveying the beaches. Tan β is the average beachface slope for all profiles measured at a certain beach. $R_{1,av}$ and $R_{2,av}$ are the run-up values derived from eqs. (2) and (3) for the average wave conditions, while $R_{1,2\%}$ and $R_{2,2\%}$ are the run-up values only exceeded by 2% of the waves. Berms refer to the number of berms observed on the different beaches.

	Beach	Area (m^2)	Length (m)	Av. Width (m)	Max. Height (m)	Av. Height (m)	Tanβ	$R_{1,av}$	$R_{2,av}$	$R_{1,2\%}$	$R_{2,2\%}$	Berms
	N1	1658	128.4	12.9	3.3	1.7	0.21	3.24	2.83	9.12	9.44	0
	N2	4057	173.2	23.4	5.0	3.0	0.35	4.17	3.64	11.67	12.10	1–2
	N3	2834	79.6	35.6	5.6	2.7	0.21	3.18	2.78	8.97	9.26	2
Delta North	N4	88	6.6	13.3	2.8	1.6	0.16	2.85	2.48	8.04	8.28	0
	S1	4245	185.7	22.9	5.4	3.2	0.31	3.90	3.40	10.95	11.32	1–2
	S2	930	35.6	26.1	4.3	1.9	0.19	3.06	2.67	8.62	8.91	2
	S3	272	30.7	8.9	1.8	1.4	0.28	3.69	3.22	10.40	10.71	0–1
	S4	2419	130.1	18.6	6.1	2.2	0.17	2.87	2.50	8.09	8.34	1–2
	S5	4024	113.2	35.5	5.8	3.2	0.23	3.40	2.96	9.59	9.86	2
	S6	1073	72	14.9	5.3	2.4	0.20	3.14	2.73	8.83	9.13	1
	S7	4937	129.4	38.2	5.8	3.0	0.25	3.52	3.07	9.94	10.21	2
	S8	319	29.7	10.7	2.6	1.5	0.23	3.39	2.96	9.57	9.84	0–1
	S9	601	48.6	12.4	1.9	1.1	0.13	2.54	2.21	7.17	7.41	0
Delta South	S10	10,066	222.4	34.9	7.1	3.7	0.27	3.65	3.18	10.27	10.58	2

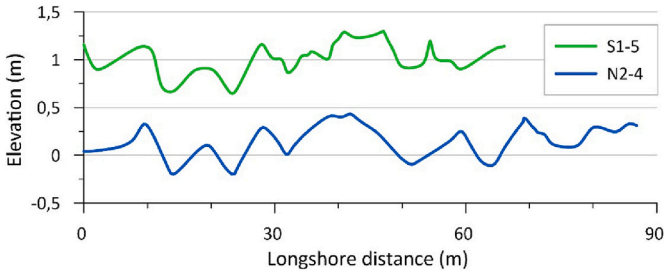

Fig. 12. Alongshore profiles at N2 and S1 beaches, corresponding to the red transects shown in Figs. 8 and 9, respectively. Note they are measured at different elevations relative to the mean sea level.

of occurring waves.

Up to two berms can be found on most of these beaches. The tidal berm is located in the upper part of the beachface. Its elevation depends on the run-up, but it generally lies at a height of 2–3 m, within the range of the run-up values obtained from the average values of H_s, T_p and T_z (Table 3). Therefore, the tidal berm is continuously swept by waves. However, $R_{2\%}$ values obtained with eqs. (2) and (3) are much higher than the maximum elevation measured in all the beaches, meaning that the beaches are fully swashed under high energy events. This explains the presence of the wood debris observed always landward the storm berm and at the inshore limit of the beach (Fig. 13 A, B). On the other hand, the high $R_{2\%}$ values obtained could be overestimated, implying that Poate et al. (2016) equations do not account properly for the water percolation through the coarse and irregular sediments forming these beaches, which promotes a decrease in uprush wave energy and a reduced run-up.

The broader beaches normally present a storm berm located landward and at a higher elevation than the tidal berm. This storm berm is normally found between 4 and 5 m height (Fig. 11). This morphological feature was identified in 7 of the 14 beaches analyzed in this work. Its development is related to beach width and high wave energy situations. All the beaches where the storm berm is present show an average width larger than 20 m, while beaches narrower than this show either 1 or no berms (Table 3). This confirms that in this type of environments the existence of a wide enough beach profile is a key factor for storm berm development. Narrower profiles do not have enough amplitude for storm berm development.

With respect to the influence of high waves, several works (Kench et al., 2017; Casamayor et al., 2022, among others) have measured the transport of pebbles and cobbles onto the upper berm under high energy conditions. In this case study, up to nine stormy events were recorded in a few months (Table 1). These high waves, associated many times to high sea level situations, yield much higher $R_{2\%}$ values (Table 3), which is determinant where the beach width is large enough to build up the storm berm and to move the wood debris onto the landward part of the beach.

5.4. Wave analysis

There are two possible wave conditions that could be responsible for the onshore transport of clasts located underwater, potentially explaining the upper beach build-up and storm berm construction on pebble beaches: conditions of very high energy waves (Kench et al., 2017; Casamayor et al., 2022) and conditions associated to swell dominance (Komar, 1998; Masselink et al., 2010). Wave propagation simulations were not conducted for this study, but large-scale wave height attenuation due to refraction processes is not expected to occur due to the narrow and steep shelf along the island.

The period between the formation of the lava deltas and the conclusion of data collection for this study was about seven months. During that period a succession of nine high wave energy events were recorded along the western coast of La Palma. The statistical approach of the 99th percentile indicates that only 1% of the year (3.65 days) is, on average, under storm conditions. During these seven months the wave height threshold was surpassed for 196 h corresponding to 8.2 days of storm conditions in the area, indicating that storminess during the period considered was much higher than normal.

There is some discrepancy in the literature regarding the role of storms in gravel beach berm formation since both erosion and accretion processes have been reported. In this context, the work by Ruiz de Alegria-Arzaburu and Masselink (2010) shows that the upper profile of a particular beach showed either erosion or accumulation depending on wave direction during storms. In their case, erosion was promoted when the storm direction was normal to the shoreline, while accretion was observed when storms presented high obliquity to the shoreline. Following this criterion, wave direction during the nine storms recorded at the study area was examined (Table 1, Fig. 17). Considering that the beaches in the study area follow a N-S direction (Fig. 1), only storms 7 and 8 present a western direction perpendicular to the coast and could generate erosion. The other 7 storms show a NW-NNW direction which implies hitting the coastline with a large approaching wave angle. This would result in building up the storm berm.

Most of the storms lasted long enough to be taking place at high tide, and some of them even occurred at spring tides (storms 5 and 8, Table 1) when wave action was able to have a much further onshore effect. Many authors (e.g., Masselink et al., 2010; Shu et al., 2019) have highlighted that when a storm overlaps with higher sea levels, its effect may result in

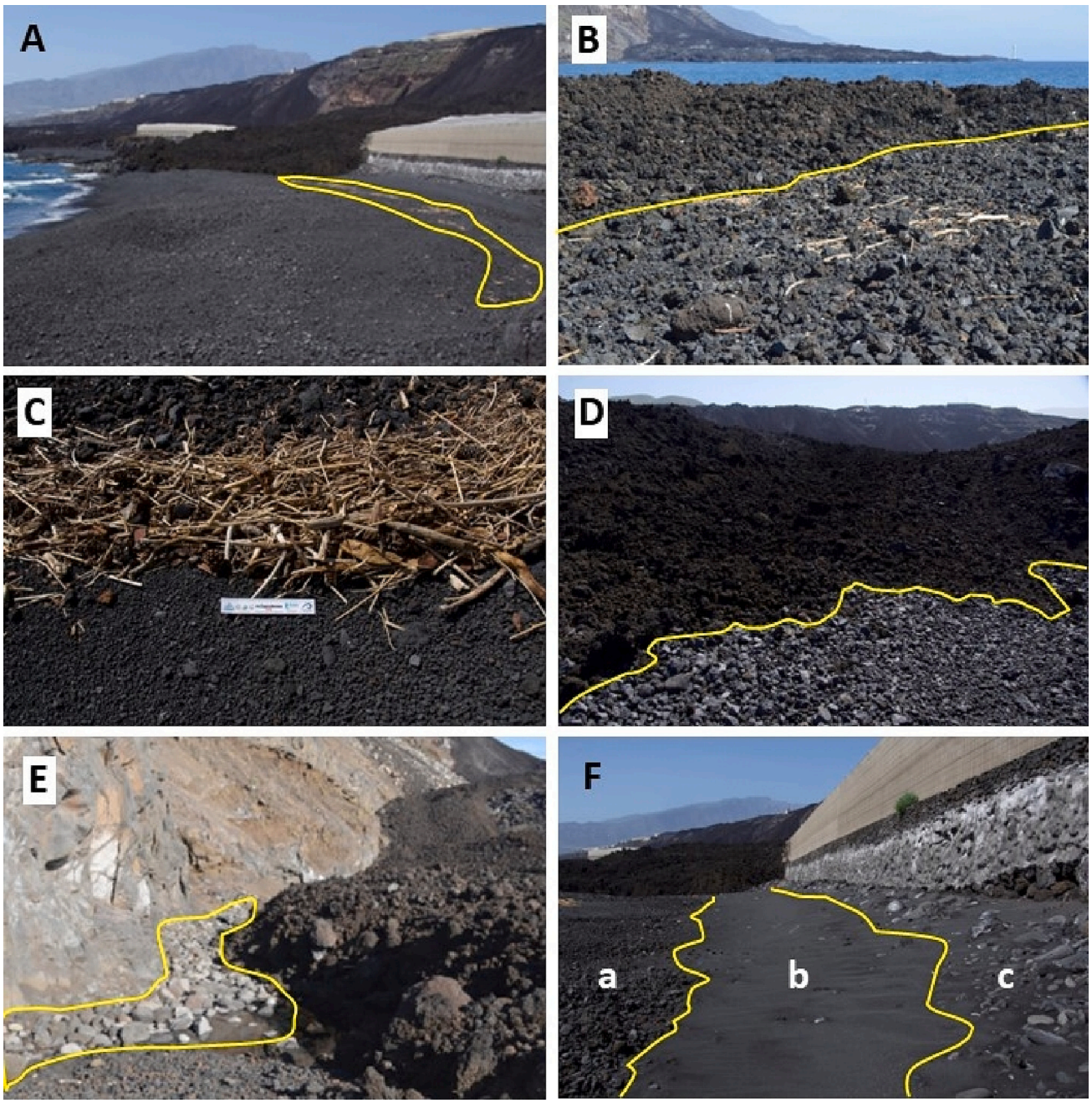

Fig. 13. A) General view of beach S10, with a wide backshore area. The wood debris deposits, distributed along the beach and landward the storm berm, are shown enclosed by a yellow line. B) Wood debris in the shoreward limit of beach N3. The yellow line shows the limit between the gravel beach deposit and the scoriaceous materials of the lava flow. C) Close-up photograph of the wood debris. The ruler scale is 30 cm long. D) Landward boundary of one of the beaches. Note the color difference between the gravel beach deposit and the none reworked scoriaceous materials of the lava flow. E) Rounded boulders next to the cliff in the SE corner of S1 beach. F) Landward limit of S10 beach. Before the eruption there was a narrower beach in this area: a) New angular pebbles; b) Strip of volcanic ash; c) Rounded cobbles and boulders from the existing beach prior to the eruption.

strong changes in beach geomorphology within a short time. Additionally, storms 1, 3, 4 and 9 are classified as classes III and IV (Table 1) following the Mendoza et al. (2011) scale.

The analysis of swell situations is important because berm construction has been reported under low wave steepness values ($H/L < 0.01$), while berm dismantling is expected under situations dominated by high steepness waves ($H/L > 0.01$) (Komar, 1998; Masselink et al., 2010).

The joint consideration of both wave criteria (wave energy and steepness), and the separation of steepness values in three regions to avoid the uncertainty of values close to $H/L = 0.01$, led us to define four possible regions. Region A is characterized by high energy waves (those defined for storm situations when $H_s > H_s$ threshold), while regions B, C and D all show low energy waves and differ according to their wave steepness values: $H/L < 0.008$; $0.008 \leq H/L \leq 0.012$ and $H/L > 0.012$ for regions B, C and D respectively (Fig. 6). Situations under A and B regions are the most favorable for onshore transport and berm construction. Equilibrium is expected under the C region, while conditions in the D region would denote offshore transport and berm erosion.

Comparison of the long-term wave climate data with the situation recorded during the seven months in which the beaches were formed shows strong differences between the two wave data series (Table 2).

Table 4
Measured and estimated sediment volume change in the beaches under study. The letter Y/N to the right of the beach number indicates whether the beach is new (Y) or if it already existed (N). Positive values are indicative of accumulation, while negative values denote erosion. The area-normalized values (in m^3/m^2) are obtained in the previously existing beaches by dividing the measured volume by the beach area (Table 3), while in the new beaches is the estimated volume divided by the beach area.

	Beach		Measured volume (m^3)	Estimated volume (m^3)	Total volume (m^3)	Normalized volume (m^3/m^2)
Delta North	N1	N	−107		−107	−0,06
	N2	N	12,351	1949	14,300	3,04
	N3	Y		1984	1984	0,70
	N4	Y		62	62	0,70
Delta South	S1	N	16,774	9212	25,986	3,95
	S2	Y		651	651	0,70
	S3	Y		190	190	0,70
	S4	Y		1693	1693	0,70
	S5	Y		2817	2817	0,70
	S6	Y		751	751	0,70
	S7	Y		3456	3456	0,70
	S8	N	433	31	465	1,36
	S9	Y		421	421	0,70
	S10	N	25,180	1220	26,400	2,50
TOTAL			54,631	24,437	79,068	
%			69.1	30.9	100	

Storm conditions are nearly 4 times more frequent in the short wave data series than in the long one. Additionally, berm build-up situations, defined by small wave steepness values ($H/L < 0.008$), are present >74% of the time during the seven-month period when these beaches formed, while these situations are only present <7% of the time in modal ocean conditions. The opposite behavior is found for high wave steepness values ($H/L > 0.012$), ranging between 4.6% and 67.8% for the short- and the long-term data series, respectively.

These figures reinforce the idea that these beaches could not have formed without the occurrence of successive NNW storms coupled with a clear dominance of long period swell waves. Both conditions contribute to the onshore transport of submerged pebbles and cobbles to the swash zone and to the berm build-up found in theses beaches.

5.5. Textural maturity and beach profile zonation

Although it is not possible to assign a single sediment size for each measured beach profile, pebbles and cobbles are the dominant sediment size in the beaches under study ($4 < D_{50} \leq 256$ mm). The beachface slope values obtained in this work lay in the range 0.11–0.57 (Fig. 11), within the range of values reported by Bujan et al. (2019), who undertook a major compilation of beachface slope values vs. grain size from previously published works.

The accumulation of woody debris at high topographic elevations and large distances from the shoreline is attributed to high waves, since wood debris represents the inland penetration of waves during storm events. Particularly in gravel-dominated beaches, Kennedy and Woods (2012) found that woody debris were deposited during storms, being positioned at the top of the storm berm. In this case, debris were found even landward of the storm berm, which can only be explained by overtopping and debris overwash at the crest of the storm berm, associated to run-up derived after storm conditions.

The differences in roundness between sediments from the beachface and from the backshore are due to the different degrees of exposure to wave abrasion. Grain shape for textural maturity is usually studied in terms of roundness (Tunwal et al., 2018), and it is generally accepted that a rise in total energy expended on sediments increases their textural maturity (Friedman and Sanders, 1978; Ehlers and Blatt, 1982). A qualitative approach to the dominant processes and clast roundness variation led us to define four different sectors in the cross-shore direction (Fig. 18):

(i) Submerged sediments within the depth of closure are abraded by wave action (Leont'yev, 2022). This abrasion process mostly depends on the rolling effect of individual particles, which are moved landwards thanks to the dominant low steepness waves. The low density of this material favors their movement.
(ii) Sediments in the swash zone up to the tidal berm are continuously reworked due to the uprush and backwash of dominant waves. Their degree of roundness and textural maturity is higher. Onshore transport of these particles normally occurs under low steepness waves.
(iii) A third zone ranges from the tidal berm to the storm berm. This area is only reached by the higher waves. Since sediments in this area are only moved during high energy events, they should not be as well-rounded as in the swash zone. Nevertheless, the storm berm is built up from clasts from the foreshore, which are already well-rounded when reaching this location. Therefore, the textural maturity should be like that of sediments from the beachface.
(iv) The fourth zone is, properly speaking, the backshore, the area landward of the storm berm. The presence of wood debris in this area indicates that the entire beaches are fully overwashed during high waves associated to high tide conditions. This area is in certain beaches highly irregular. The topographic irregularities observed on the backshore of N3 and S5 beaches (Figs. 8 and 9) could be due to the presence of underlying lava flows that become covered by cobble-sized particles. However, this is speculative as it is not known what lies below the surface rock fragments.

Clasts in this area come from two sources. The first source is the natural dismantling of the adjacent volcanic materials after the episodic storms that hit the area during the high tide periods. These breccia fragments have been slightly reworked. They are brownish and highly irregular, with larger indentations and sharp boundaries. The second source are clasts that have been pulled by the northern storms from the above-mentioned zones. The quick accumulation does not allow these particles to become rounded. They can be differentiated from the inland lava fragments because these are greyish and their edges slightly smoothed (Fig. 13B, D). Overall, the textural maturity in the backshore is much lower than in the previous zones.

5.6. Beach evolution

All the beaches considered in this study (except N1) show a very fast evolution. The ones that already existed before the eruption have accumulated around 67,000 m^3 of new sediment, which implies reaching higher elevation and width. Such fast growth is due to the location of most of them at the lateral limits of the lava deltas, which represent a

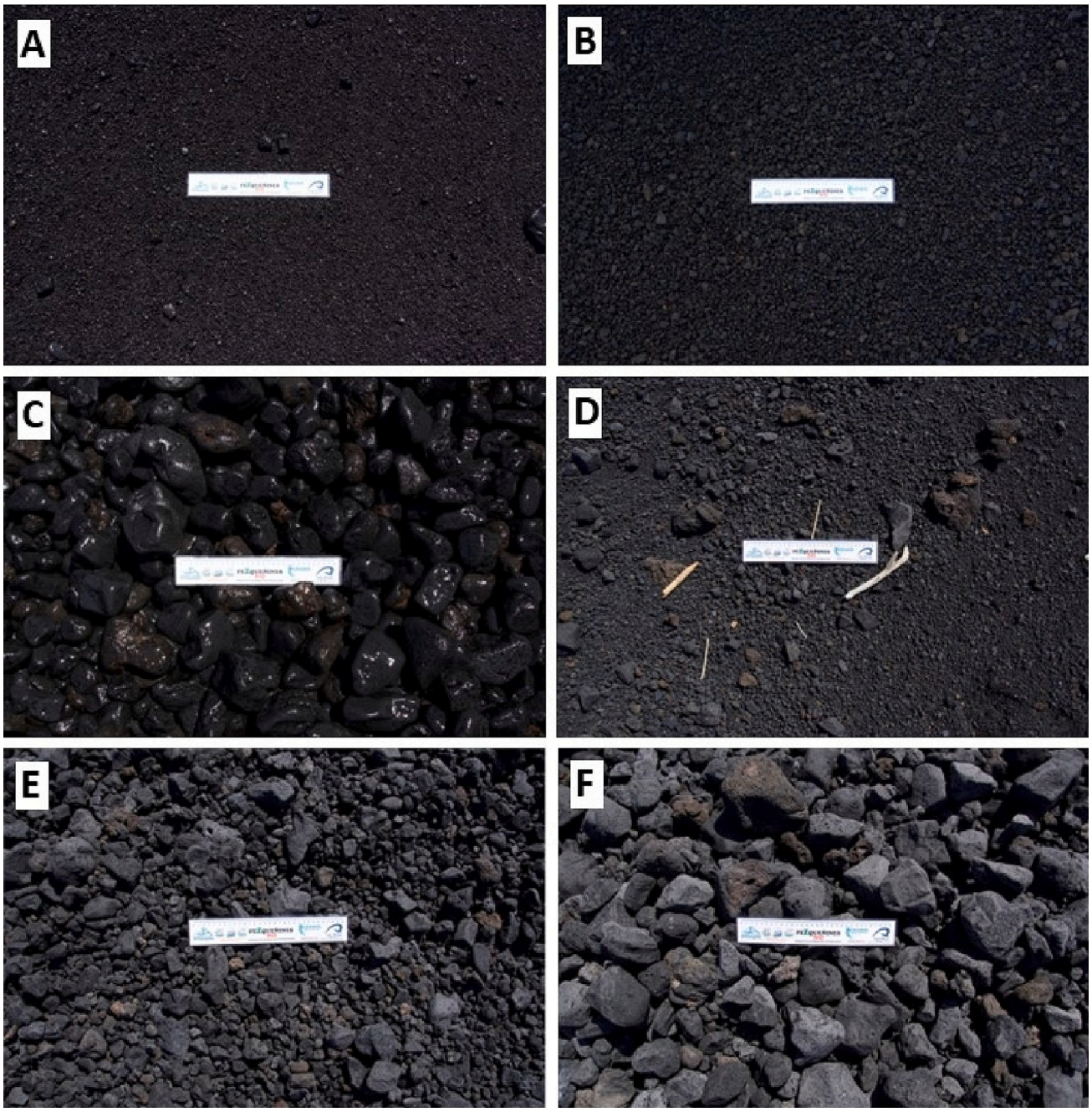

Fig. 14. Close-up view of different types of sediments. In all cases the scale used is a 30 cm long ruler. A) Moderately well-sorted coarse sands from the beachface, beach S5. B) Well-sorted gravels from the beachface, beach S3. C) Well-sorted, moderately rounded cobbles from a steep foreshore, southern end of beach S10. D) Poorly-sorted gravels from the landward limit of the backshore, beach S5. Note the presence of sparce debris. E) Poorly-sorted and highly angular pebbles from the upper berm, beach S5. F) Angular cobbles from the backshore, beach S5. Location of each image is shown in Figs. 9 and 10.

natural boundary that favors the accumulation of sediments by interrupting the longshore drift associated to NNW storms and creating a more sheltered area. Additionally, in these areas the bathymetry is not too steep, so that they could become wider as they receive new sedimentary material. Nevertheless, the arrival of additional significant volumes of sediments is not expected to occur, which is related to the greater distance to the lava deltas.

On the other hand, newly formed beaches have been formed because of the erosion of the frontal part of the lava deltas and the onshore transport of clasts located underwater within the closure depth. In this case, the boundary conditions are not favorable for beach formation and eventual growth since there is a lack of lateral structures and the bathymetry is much steeper. However, the arrival of newer sediments is nearly ensured since the source area comprises the limits of each of these beaches. Nonetheless, these beaches may continue to grow and some new ones may develop depending on the continuance of northern high wave energy events that will gradually erode and dismantle the lava delta front, coupled with dominant conditions of low steepness waves.

The future evolution of these beaches will be conditioned by wave climate. If it reverts to the modal conditions where high wave steepness values are dominant (Table 2) as well as to situations where the storms approach from the west, the beaches studied in this work could show strong erosion, and eventually the smaller ones could even disappear.

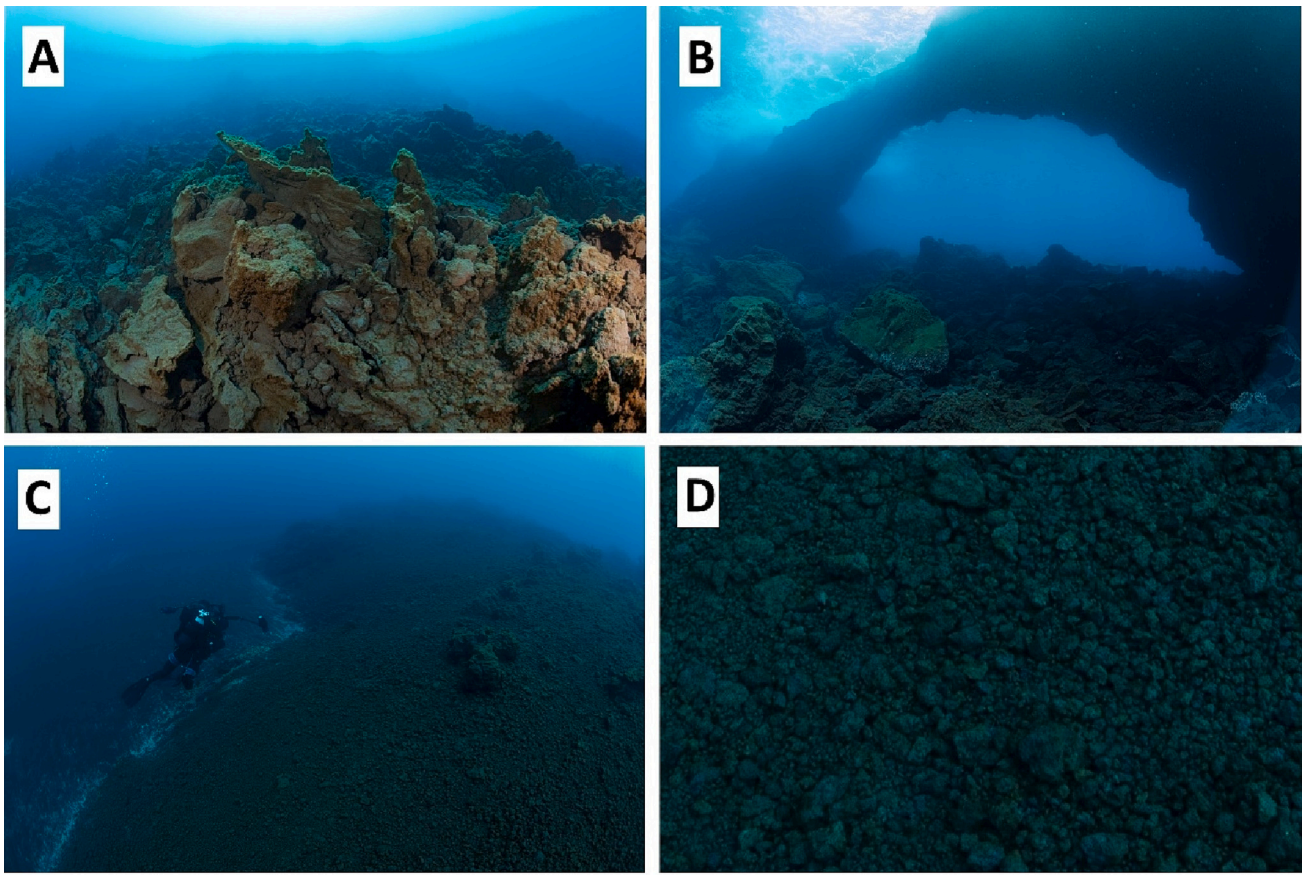

Fig. 15. Photographs of different aspects of the submarine apron of the lava deltas. A) General aspect of the scoriaceous lava flows. B) Rocky arc at about 6 m depth. Note the broken fragments at the front. C) Submarine accumulation of coarse-grained scoria fragments (≈5–20 m depth). D) Close-up view of the scoria fragments at ≈5 m depth. Note the irregularity and the slightly rounded edges of clasts due to wave-induced rolling.

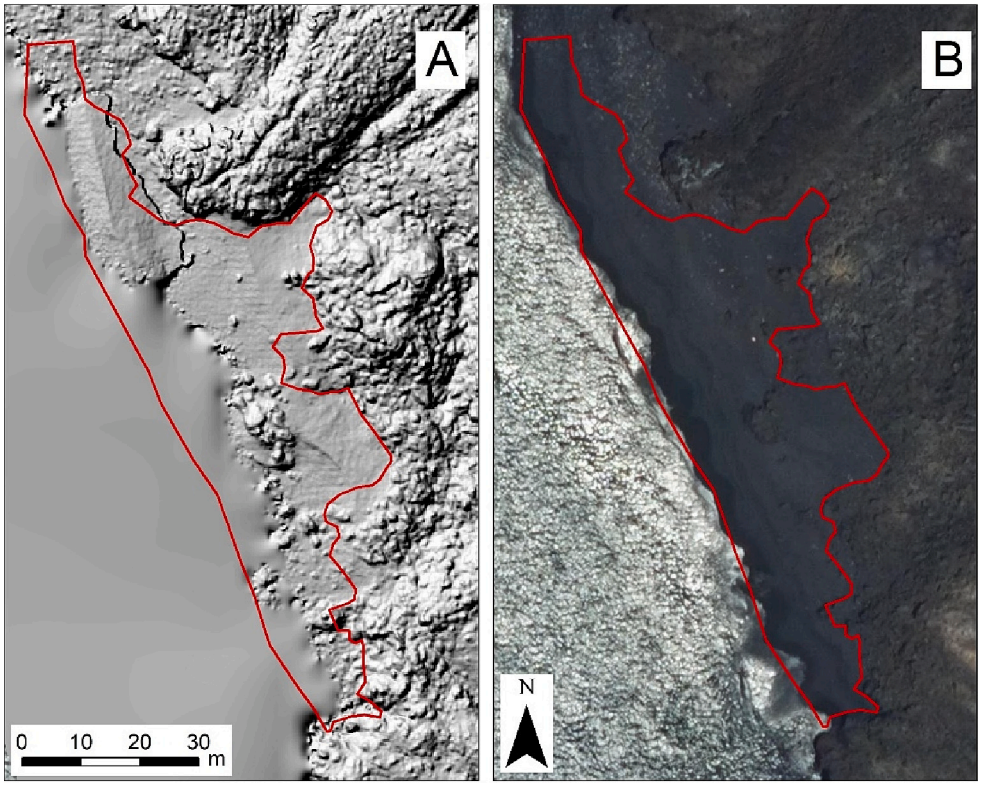

Fig. 16. Comparison of beach S4 between December 2021 (A) and May 2022 (B). Note the presence of large rocks in A that have been washed out in B and the beach cusp at the southern end. The red contour represents the limits of this beach as it was topographically surveyed in this work. (A) Hillshade digital model derived from the 2021 DEM. (B) Orthophoto from www.idecanarias.es. (For interpretation of the references to color in this figure legend, the reader is referred to the web version of this article.)

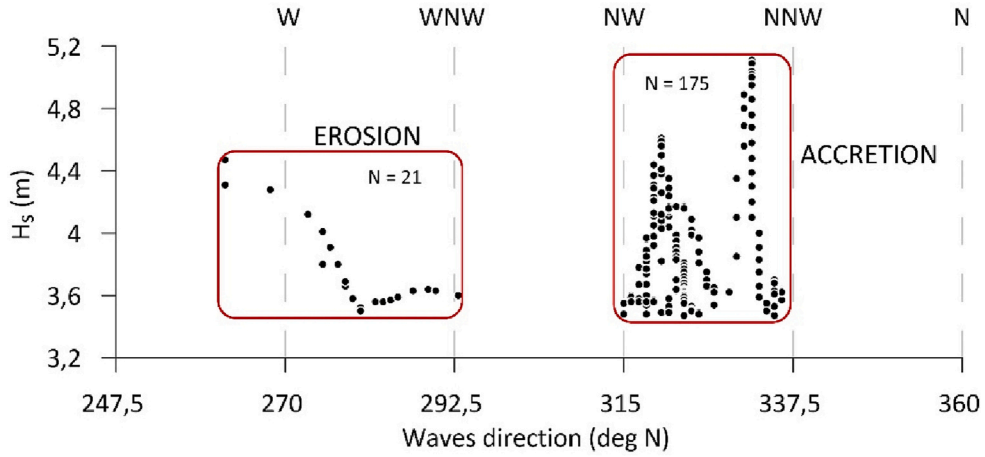

Fig. 17. Directional variability of the storms wave data. Only data above the H_s threshold are plotted. The resultant process (erosion/accretion) and number of data points is shown.

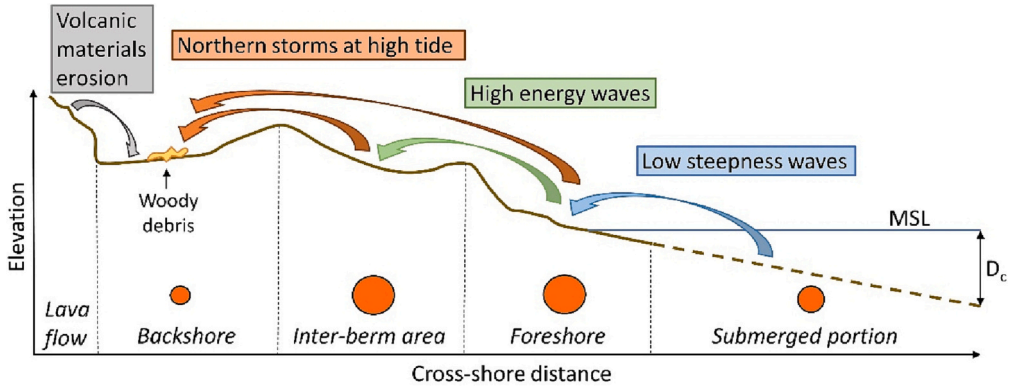

Fig. 18. Schematic representation of a characteristic beach profile, with the four zones defined. It shows the main driving mechanisms that contribute to building up each zone. Larger circles indicate higher textural maturity.

6. Conclusions

The development of new beaches associated to volcanic environments is examined in this paper. Thirteen beaches formed within a few months of the arrival of several lava flows to the ocean and the subsequent formation of two lava deltas in La Palma Island. About 79,000 m^3 of volcanic rock fragments that came from two main source areas developed these beaches: *(i)* the erosion and gradual dismantling of the lava delta fronts by wave action, generating volcanic clasts that became incorporated in the beaches; and *(ii)* large deposits of low-density scoria fragments located underwater at several meters depth. Where these deposits are located within the depth of closure can be moved onshore by low steepness waves. Additional sources, such as the aerial deposition of volcanic ash and pyroclasts, as well as cliff rock falls, are almost negligible. The sediments accumulated on these beaches are highly vesiculated and irregular volcanic clasts, with the dominant size being pebbles and cobbles together with some sparce patches of coarse sand and gravels.

Up to nine wave storm events took place during the seven months between the beginning of the formation of the lava deltas and the conclusion of the collection of data for this study. Six of them can be considered major storms, either because they correspond to classes III and IV of the Mendoza et al. (2011) scale or because of their concurrence with spring tides, when high water levels involve a much greater landward wave effect. Furthermore, seven of these storms hit the coastline from the NNW, with a large approaching wave angle. The role of these storms, coupled with the dominance of very low steepness waves, was crucial in the formation of these beaches, allowing the onshore transport of submarine clasts and the build-up of the storm berm. The morphological characteristics of these beaches can be summarized as follows:

- Beachface slope values within the range 0.11–0.57, similar to other beaches with similar grain size.
- A tidal berm at 2–3 m elevation, within the action of the run-up obtained from average wave conditions.
- A landward storm berm at 4–5 m elevation, reached by high energy waves. This storm berm is overpassed when such waves occur during high tide conditions.
- The occurrence of wood debris in the backshore, shoreward of the storm berm, indicating that the whole beach can be fully overwashed.
- Cusp-like morphologies are a common feature along the foreshore.

The wave climate was responsible for the two different patterns found in the beaches. Firstly, beaches that already existed prior to the eruption experienced a net accumulation of about 67,000 m^3 of clasts, with a subsequent increment in amplitude and height. Secondly, the newly formed beaches account for some 12,000 m^3 as a consequence of the dismantling of the lava delta front and later accumulation of the resultant volcanic clasts.

Significant differences in roundness were found between clasts from the submerged profile, the swash zone, the storm berm and the backshore. These changes indicate that particle irregularities and edge smoothing evolve with the degree of exposure to wave action. Therefore,

the textural maturity of the particles shows strong changes in the cross-shore direction, related to the driving mechanisms responsible for the development of these newly formed environments, which are still under construction.

Finally, the future evolution of these beaches will depend on the differences in boundary conditions between previously existing and newly formed beaches and on the wave climate, which is the main forcing agent responsible for erosion/accumulation processes on the beaches.

Credit authorship contribution statement

Conceptualization and original draft of the manuscript by I. Alonso; F. Santana-Sarmiento and F. Andrés-Araujo carried out the field topographic measurements; I. Alonso, M. Casamayor, M. J. Sánchez-García, I. Montoya-Montes and A. Brenes did the sediment sampling and data analysis; R. Herrera performed the submarine identification. All co-authors provided their critical reviews of the document.

Declaration of Competing Interest

The authors declare that they have no known competing financial interests or personal relationships that could have appeared to influence the work reported in this paper.

Data availability statement

The topographic data that support the findings of this study are stored in the Zenodo repository and are available at https://doi.org/10.5281/zenodo.7054504. The wave data are available at https://www.puertos.es/es-es/oceanografia

Acknowledgements

The contribution of PLOCAN by facilitating access to the beaches on both lava deltas is greatly appreciated, with particular thanks going to Gabi, the captain of the boat. We thank the Canary Islands Territorial Information System (SITCAN for its initials in Spanish) from GRAFCAN – Canary Islands Government, for allowing access to the 2020 LiDAR data used in this work. This research was supported by the MESVOL research project, funded by the Spanish Ministry of Science and Innovation. We finally thank helpful comments from the Journal Editor and two anonymous Reviewers.

References

Ancochea, E., Hernan, F., Cendrero, A., Cantagrel, J.M., Fuster, J.M., Ibarrola, E., Coello, J., 1994. Constructive and destructive episodes in the building of a young oceanic island, La Palma, Canary Islands, and the genesis of the Caldera de Taburiente. J. Volcanol. Geotherm. Res. 60, 243–262. https://doi.org/10.1016/0377-0273(94)90054-X.

Banda, E., Ansorge, J., Dañobeitia, J.J., Suriñach, E., 1981. Features of crustal structure under the Canary Islands. Earth Planet. Sci. Lett. 55 (1), 11–24. https://doi.org/10.1016/0012-821X(81)90082-0.

Bertoni, D., Sarti, G., Benelli, G., Pozzebon, A., Raguseo, G., 2010. Radio Frequency Identification (RFID) technology applied to the definition of underwater and subaerial coarse sediment movement. Sediment. Geol. 228 (3), 140–150. https://doi.org/10.1016/j.sedgeo.2010.04.007.

Bertoni, D., Dean, S., Trembanis, A.C., Sarti, G., 2020. Multi-month sedimentological characterization of the backshore of an artificial coarse-clastic beach in Italy. Rendiconti Lincei. Sci. Fisiche Nat. 31, 65–77. https://doi.org/10.1007/s12210-019-00852-2.

Brayne, R.P., Lorang, M.S., Naylor, L.A., Reinhardt, L., 2020. Field-based observation of the entrainment threshold of cobbles with motion loggers. J. Coast. Res. 95, 392–397. https://doi.org/10.2112/SI95-076.1.

Bujan, N., Cox, R., Masselink, G., 2019. From fine sand to boulders: Examining the relationship between beach-face slope and sediment size. Mar. Geol. 417, 106012 https://doi.org/10.1016/j.margeo.2019.106012.

Calvet, F., Cabrera, M.C., Carracedo, J.C., Mangas, J., Pérez-Torrado, F.J., Recio, C., Travé, A., 2003. Beachrocks from the island of La Palma (Canary Islands, Spain). Mar. Geol. 197 (1), 75–93. https://doi.org/10.1016/S0025-3227(03)00090-2.

Carracedo, J.C., Rodriguez-Badiola, E., Guillou, H., de la Nuez Pestana, J., Pérez Torrado, F.J., 2001. Geology and volcanology of La Palma and El Hierro, Western Canaries. Estud. Geol. 57 (5–6), 175–273. https://doi.org/10.3989/egeol.01575-6134.

Casamayor, M., Alonso, I., Valiente, N.G., Sánchez-García, M.J., 2022. Seasonal response of a composite beach in relation to wave climate. Geomorphology 408, 108245. https://doi.org/10.1016/j.geomorph.2022.108245.

Detert, M., Weitbrecht, V., 2013. User guide to gravelometric image analysis by Basegrain. In: Fukuoka, S., Nakagawa, H., Sumi, T., Zhang, H. (Eds.), Advances in Science and Research. Taylor and Francis Group, London, pp. 1789–1796.

Dorsch, W., Newland, T., Tassone, D., Tymons, S., Walker, D., 2008. A Statistical Approach to Modelling the Temporal patterns of Ocean Storms. J. Coast. Res. 246, 1430–1438. https://doi.org/10.2112/07-0847.1.

Ehlers, E.G., Blatt, H., 1982. Petrology: Igneous, Sedimentary, and Metamorphic. W.H. Freeman and Company, San Francisco, CA, p. 732.

del Estado, Puertos, 2019. Red de mareógrafos de Puertos del Estado (REDMAR). Puerto de Santa Cruz de La Palma. Technical report. Available online: https://bancodatos.puertos.es/BD/informes/globales/GLOB_2_3_3465.pdf (accessed on 08 November 2022).

del Estado, Puertos, 2020. Conjunto de datos SIMAR. Technical report. Available online: https://bancodatos.puertos.es/BD/informes/INT_8.pdf (accessed on 20 May 2022).

del Estado, Puertos, 2022. Clima medio de oleaje. Nodo SIMAR 4006016. Available online: https://bancodatos.puertos.es/BD/informes/medios/MED_1_8_4006016.pdf (accessed on 25 October 2022).

Fan, L., Smethurst, J., Atkinson, P., Powrie, W., 2014. Propagation of vertical and horizontal source data errors into a TIN with linear interpolation. Int. J. Geogr. Inf. Sci. 28 (7), 1378–1400. https://doi.org/10.1080/13658816.2014.889299.

Friedman, G.M., Sanders, J.E., 1978. Principles of Sedimentology. John Wiley & Sons, New York, NY, p. 792.

Gonçalves, M., Martinho, P., Guedes, Soares C., 2020. Wave energy assessment based on a 33-year hindcast for the Canary Islands. Renew. Energy 152, 259–269. https://doi.org/10.1016/j.renene.2020.01.011.

González, P.J., 2022. Volcano-tectonic control of Cumbre Vieja. Science 375 (6587), 1348–1349. https://doi.org/10.1126/science.abn51.

Guerra-Medina, D., Rodríguez, G., 2021. Spatiotemporal Variability of Extreme Wave Storms in a Beach Tourism Destination Area. Geosciences 11, 237. https://doi.org/10.3390/geosciences11060237.

Hallermeier, R.J., 1981. A profile zonation for seasonal sand beaches from wave climate. Coast. Eng. 4, 253–277. https://doi.org/10.1016/0378-3839 (80)90022-8.

Harley, M., 2017. Coastal storm definition. In: Coco, G., Ciavola, P. (Eds.), Coastal Storms. John Wiley & Sons, Ltd, Chichester, UK, pp. 1–21. https://doi.org/10.1002/9781118937099.ch1.

Horn, D., Li, L., 2006. Measurement and modelling of gravel beach groundwater response to wave run-up: effects on beach profile changes. J. Coast. Res. 22 (5), 1241–1249. https://doi.org/10.2112/06A-0006.1.

Jennings, R., Shulmeister, J., 2002. A field based classification scheme for gravel beaches. Mar. Geol. 186 (3–4), 211–228. https://doi.org/10.1016/S0025-3227(02)00314-6.

Kench, P.S., Beetham, E., Bosserelle, C., Kruger, J., Pohler, S.M.L., Coco, G., Ryan, E.J., 2017. Nearshore hydrodynamics, beach face cobble transport and morphodynamics on a Pacific atoll motu. Mar. Geol. 389, 17–31. https://doi.org/10.1016/j.margeo.2017.04.012.

Kennedy, D.M., Woods, J.L.D., 2012. The influence of coarse woody debris on gravel beach geomorphology. Geomorphology 159–160, 106–115. https://doi.org/10.1016/j.geomorph.2012.03.009.

Komar, P.D., 1998. Beach Processes and Sedimentation. Prentice-Hall, Englewood Cliffs, New Jersey.

Kraus, N.C., Larson, M., Wise, R.A., 1998. Depth of Closure in Beach-fill Design. In: Coastal Engineering Technical Note CETN II-40, 3/98, U.S. Army Engineer Waterways Experiment Station, Vicksburg, MS.

Leont'yev, I.O., 2022. Abrasion of Coast Composed of Loose Material. Oceanology 62, 105–113. https://doi.org/10.1134/S0001437022010088.

Marrero, N., Montoya, I., Alonso, I., 2017. Evolución de la línea de costa de Tazacorte entre 1964 y 2015 (La Palma, Islas Canarias). Geotemas 17, 247–250.

Masselink, G., Li, L., 2001. The role of swash infiltration in determining the beachface gradient: a numerical study. Mar. Geol. 176 (1–4), 139–156. https://doi.org/10.1016/S0025-3227(01)00161-X.

Masselink, G., Russell, P., Blenkinsopp, C., Turner, I., 2010. Swash zone sediment transport, step dynamics and morphological response on a gravel beach. Mar. Geol. 274 (1–4), 50–68. https://doi.org/10.1016/j.margeo.2010.03.005.

Masson, D.G., Watts, A.B., Gee, M.J.R., Urgeles, R., Mitchell, N.C., Le Bas, T.P., Canals, M., 2002. Slope failures on the flanks of the western Canary Islands. Earth Sci. Rev. 57 (1–2), 1–35. https://doi.org/10.1016/S0012-8252(01)00069-1.

McGlashan, D.J., Duck, R.W., Reid, C.T., 2005. Defining the foreshore: coastal geomorphology and British laws. Estuar. Coast. Shelf Sci. 62 (1), 183–192. https://doi.org/10.1016/j.ecss.2004.08.016.

Mendoza, E.T., Jimenez, J.A., Mateo, J., 2011. A coastal storms intensity scale for the Catalan Sea (NW Mediterranean). Nat. Hazards Earth Syst. Sci. 11 (9), 2453–2462. https://doi.org/10.5194/nhess-11-2453-2011.

Morton, I.D., Bowers, J., Mould, G., 1997. Estimating return period wave heights and wind speeds using a seasonal point process model. Coast. Eng. 31, 305–326. https://doi.org/10.1016/s0378-3839(97)00016-1.

Palanco, S., Pérez-López, R., Galindo-Jiménez, I., Bernal, A., Aranda, S., López-Escalante, M.C., Leinen, D., Mediato, J.F., López-Gutiérrez, J., Ramos-Barrado, J.R., 2022. Field deployment of a man-portable stand-off laser-induced breakdown spectrometer: a preliminary report on the expedition to the Cumbre Vieja volcano

(La Palma, Spain, 2021). Spectrochim. Acta B At. Spectrosc. 190, 106391 https://doi.org/10.1016/j.sab.2022.106391.
Pedrozo-Acuña, A., Simmonds, D.J., Otta, A.K., Chadwick, A.J., 2006. On the cross-shore profile change of gravel beaches. Coast. Eng. 53 (4), 335–347. https://doi.org/10.1016/j.coastaleng.2005.10.019.
Pilar, P., Guedes Soares, C., Carretero, J.C., 2008. 44-year wave hindcast for the North East Atlantic European coast. Coast. Eng. 55 (11), 861–871. https://doi.org/10.1016/j.coastaleng.2008.02.027.
Poate, T.G., McCall, R.T., Masselink, G., 2016. A new parameterisation for runup on gravel beaches. Coast. Eng. 117, 176–190. https://doi.org/10.1016/j.coastaleng.2016.08.003.
Pontee, N.I., Pye, K., Blott, S., 2004. Morphodynamic behaviour and sedimentary variation of mixed sand and gravel beaches, Suffolk. UK. J. Coastal Res. 20, 256–276. https://www.jstor.org/stable/4299281.
Reis, A.H., Gama, C., 2010. Sand size versus beachface slope – an explanation based on the constructal law. Geomorphology 114 (3), 276–283. https://doi.org/10.1016/j.geomorph.2009.07.008.
Richmond, B.M., Watt, S., Buckley, M., Jaffe, B.E., Gelfenbaum, G., Morton, R.A., 2011. Recent storm and tsunami coarse-clast deposit characteristics, southeast Hawai'i. Mar. Geol. 283 (1–4), 79–89. https://doi.org/10.1016/j.margeo.2010.08.001.
Romagnoli, C., Mancini, F., Brunelli, R., 2006. Historical shoreline changes at an active Island Volcano: Stromboli, Italy. J. Coast. Res. 22 (4), 739–749. https://doi.org/10.2112/05-0554.1.
Román, A., Tovar-Sánchez, A., Roque-Atienza, D., Huertas, I.E., Caballero Fraile-Nuez, I. E., Navarro, G., 2022. Unmanned aerial vehicles (UAVs) as a tool for hazard assessment: the 2021 eruption of Cumbre Vieja volcano, La Palma Island (Spain). Sci. Total Environ. 843, 157092 https://doi.org/10.1016/j.scitotenv.2022.157092.
Romero, J.E., Burton, M., Cáceres, F., Taddeucci, J., Civico, R., Ricci, T., Pankhurst, M.J., Hernández, P.A., Bonadonna, C., Llewellin, E.W., Pistolesi, M., Polacci, M., Solana, C., D'Auria, L., Arzilli, F., Andronico, D., Rodríguez, F., Asensio-Ramos, M., Martín-Lorenzo, A., Hayer, C., Scarlato, P., Perez, N.M., 2022. The initial phase of the 2021 Cumbre Vieja ridge eruption (Canary Islands): products and dynamics controlling edifice growth and collapse. J. Volcanol. Geotherm. Res. 431, 107642 https://doi.org/10.1016/j.jvolgeores.2022.107642.
Ruiz de Alegria-Arzaburu, A., Masselink, G., 2010. Storm response and beach rotation on a gravel beach, Slapton Sands, U.K. Mar. Geol. 278 (1–4), 77–99. https://doi.org/10.1016/j.margeo.2010.09.004.
Salvadori, G., Tomasicchio, G.R., D'Alessandro, F., Lusito, L., Francone, A., 2020. Multivariate Sea storm hindcasting and design: the isotropic buoy-ungauged generator procedure. Sci. Rep. 10, 1–12. https://doi.org/10.1038/s41598-020-77329-y.
Schneider, C.A., Rasband, W.S., Eliceiri, K.W., 2012. NIH image to ImageJ: 25 years of image analysis. Nat. Methods 9, 671–675. https://doi.org/10.1038/nmeth.2089.
Shu, F., Cai, F., Qi, H., Liu, J., Lei, G., Zheng, J., 2019. Morphodynamics of an Artificial Cobble Beach in Tianquan Bay, Xiamen, China. J. Ocean Univ. China 18 (4), 868–882. https://doi.org/10.1007/s11802-019-3860-3.
Shulmeister, J., Kirk, R.M., 1997. Holocene fluvial–coastal interactions on a mixed sand and sand and gravel beach system, North Canterbury, New Zealand. Catena 30, 337–355. https://doi.org/10.1016/S0341-8162(97)00013-1.
Tunwal, M., Mulchrone, K.F., Meere, P.A., 2018. Quantitative characterization of grain shape: Implications for textural maturity analysis and discrimination between depositional environments. Sedimentology 65 (5), 1761–1776. https://doi.org/10.1111/sed.12445.
Urgeles, R., 1999. Recurrent large-scale landsliding on the west flank of La Palma, Canary Islands. J. Geophys. Res. Solid Earth 104 (B11), 25333–25348. https://doi.org/10.1029/1999JB900243, 1999JB900243.
Voropayev, S.I., Roney, J., Boyer, D.L., Fernando, H.J.S., Houston, W.N., 1998. The motion of large bottom particles (cobbles) in a wave-induced oscillatory flow. Coast. Eng. 34, 197–219. https://doi.org/10.1016/S0378-3839(98)00019-2.
Yanes Luque, A., Rodríguez-Báez, J.A., Máyer Suárez, P., Dorta Antequera, P., López-Díez, A., Díaz-Pacheco, J., Pérez-Chacón, E., 2021. Marine storms in coastal tourist areas of the Canary Islands. Nat. Hazards 109 (1), 1297–1325. https://doi.org/10.1007/s11069-021-04879-3.